The Schwinger Model: Spectrum, dynamics and quantum quenches

A DISSERTATION PRESENTED
BY
MATEO RESTREPO A.
TO
THE PHYSICS DEPARTMENT

IN PARTIAL FULFILLMENT OF THE REQUIREMENTS
FOR THE DEGREE OF
MASTER IN SCIENCE
IN THE SUBJECT OF
PHYSICS

UNIVERSIDAD DE LOS ANDES
BOGOTÁ, COLOMBIA

NOVEMBER 2018

Thesis advisor: Andrés F. Reyes-Lega Mateo Restrepo A.

The Schwinger Model: Spectrum, dynamics and quantum quenches

Abstract

English

Quantum electrodynamics in two dimensions (one spatial dimension + time) with Dirac fermions was a model first studied by Julian Schwinger in 1962 and thus it was coined the Schwinger model. The massless model is completely solvable and shows very interesting physical phenomena such as a chiral anomaly, a massive boson generated via a kind of dynamical Higgs mechanism, the presence of confinement analogous to quark confinement in QCD_4 and spontaneous symmetry breaking of a $U(1)$ axial symmetry. The Schwinger model is the simplest gauge theory being completely solvable, thus, it is a rich toy model for studying more complex gauge theories.

In this work, we quantize the Schwinger model using Hamiltonian quantization in the temporal Weyl gauge ($A0 = 0$) which then can be written as a lattice system of spins using Kogut-Susskind fermions and a Jordan-Wigner transformation. This lattice model is numerically studied using exact diagonalization methods. We study the ground state energy, the first few excited states energies, the existence of a gap and the order parameter values both in the free massless and massive model. Additionally, we explore the dynamical evolution of the spectrum of the Dirac operator, the dynamics of the ground state and the behavior of order parameters such as the chiral condensate density as a consequence of the introduction of global quenches in the system in both the massless and the massive interacting models in the presence of a background electric field.

Español

La electrodinámica cuántica en dos dimensiones (una dimensión espacial + tiempo) con fermiones de Dirac es un modelo que estudió por primera vez Julian Schwinger en 1962, y por lo tanto se conoce como el modelo de Schwinger. El modelo sin masa es completamente soluble y exhibe fenómenos físicos muy interesantes como lo son una anomalía quiral, un bosón masivo generado por un tipo de mecanismo de Higgs dinámico, presencia de confinamiento análogo al confinamiento de los

quarks en QCD_4 y el rompimiento espontáneo de una simetría $U(1)$ axial. El modelo de Schwinger es la teoría gauge más simple, y por lo tanto, es un modelo de juguete muy útil para el estudio de teorías gauge más complejas.

En este trabajo, cuantizamos el modelo usando cuantización Hamiltoniana en el gauge temporal de Weyl ($A_0 = 0$), y posteriormente escribimos el modelo como una cadena de espines usando fermiones de Kogut-Susskind y una transformación de Jordan-Wigner. Este modelo discreto se estudia numéricamente usando métodos de diagonalización exacta. Estudiamos la energía del estado base, las energías de unos pocos estados excitados, la existencia de un gap en el espectro y parámetros de orden tanto en el modelo libre sin masa como en el modelo masivo. Adicionalmente, exploramos la dinámica del espectro del operador de Dirac, la dinámica del estado base y el comportamiento de parámetros de orden como la densidad del condensado quiral como consecuencia de la introducción de un quench global tanto en el modelo no-masivo como en el modelo masivo e interactuante en presencia de un campo eléctrico de fondo.

Contents

1 The continuum Schwinger model **1**

1.1 Motivation and Introduction 1

1.2 Lagrangian, Hamiltonian and equations of motion 3

1.2.1 The Schwinger model in a Background electric field . . 8

1.3 Chiral anomaly in the path integral formalism 11

1.3.1 Path integrals and the Grassman Jacobian 11

1.3.2 Dirac operator mode regularization 15

1.3.3 Schwinger-Dyson equation for a gauge symmetry . . . 17

1.4 Anomaly, index and topology 20

1.4.1 Zero-modes and index of the Dirac operator 20

1.4.2 Atiyah-Singer index theorem 22

1.5 Anomaly and the fermion spectrum 23

1.5.1 Schwinger model on a circle 23

1.5.2 Infrared and ultraviolet behavior 27

1.6 Comments and conclusion 31

2 Spin chains **34**

2.1 Motivation and Introduction 34

2.2 The XY-model in a transverse field 36

2.2.1 The ground state 40

2.2.2 The Phase Diagram 40

2.3 The XX-model 42

2.4 Comments and conclusion 44

3 The Schwinger model in a lattice **46**
3.1 Motivation and Introduction 46
3.2 Lattice formulation 47
3.2.1 Spin Hamiltonians 50
3.2.2 Electric field operators and Hilbert space 53
3.2.3 The background field in the lattice 54
3.2.4 Gauss law 56
3.3 Effective mass and Coulomb interaction 59
3.4 Comment and conclusion 63

4 Simulations of the Schwinger model **66**
4.1 Motivations and introduction 66
4.2 A comment on exact diagonalization 67
4.3 The free massless Schwinger model 68
4.4 The free massive Schwinger model 71
4.5 The interacting Schwinger Model 76
4.6 Quantum quenches in the Schwinger model 81
4.6.1 Quenches from the free model 84
4.6.2 Quenches between background fields 85
4.7 Comments and conclusion 87

5 Discussion and outlook **90**

References **94**

List of figures

1.2.1 Two distinct configurations for particle-antiparticle pairs in one spatial dimension. 9
1.2.2 Plot of energy density as a function of $\mathcal{E}_0$. 10
1.5.1 Fermion spectrum as function of A_1. 26

2.2.1 Phase diagram of the XY-model for γ and g positive. 41
2.3.1 $N = 24$ XX-model spectrum for $g = 1/2$ and $J = 1$. The orange dots are filled Dirac sea states of the ground state. 43

3.2.1 Lattice with open and periodic boundary condition. 48
3.2.2 Lattice of $N = 6$ spins with the values of electric field L_n fixed by Gauss's law. 57
3.3.1 Plot of effective mass term due to the background field $\mathcal{E}_0$ for $N = 5$ and $N = 25$. 60
3.3.2 Plot of effective mass term, m_ξ, for $N = 5$ and $N = 25$. 61
3.3.3 Plot of Coulomb strength interaction C_{nm} between spins in the lattice for $N = 5$ and $N = 25$. 62

4.3.1 Full spectrum of the Hamiltonian in real space. (A) Spectrum for $N = 14$ taking batches of 8 eigenvalues to show the spectrum structure and avoid clutter. (B) Single particle excitation spectrum for $N = 33$. 69

4.3.2 Ground state energy per site for $N \in [4, 24]$ for even and odd number of particles. The dashed black line is the result in the thermodynamic limit where $E_0/N = -1/\pi$ 70
4.3.3 Plot of the ground state and the first two excited states energy densities versus the inverse of the number of sites squared with $N \in [4, 22]$. Normalization of the energy density with m is made to preserve the y scale. (A) Even number of particles. (B) Odd number of particles. A linear fit is made to determine numerically the ground state energy 71
4.4.1 Plot of the spectrum in real space for different values of the mass taking batches of 5 eigenvalues. (A) $m = 2$, (B) $m = 4$, (C) $m = 6$ and (D) $m = 10$. 72
4.4.2 Plot of the ground state and the first two excited states energy densities versus the inverse of the number of sites squared with $N \in [4, 18]$ and N even. Normalization of the energy density with m is made to preserve the y scale. (A) $m = 2$, (B) $m = 4$, (C) $m = 6$ and (D) $m = 12$. 73
4.4.3 Spectrum gap energy as a function of mass 76
4.5.1 Plot of the ground state energy density for the massless interacting Schwinger model. 77
4.5.2 Plot of the density of chiral condensate as a function of q_e, $q_e \in [0, 25]$. (A) Massless case $m = 0$. (B) Massive Case $m = 2.0$. . . 78
4.5.3 Plot of the axial fermion density as a function of q_e, $q_e \in [0, 25]$ for different background field values. (A) Massless case $m = 0$. (B) Massive Case $m = 2.0$. 79
4.5.4 Plot of the order parameters as a function of fermion mass $m \in [0, 1]$ for different background field values.The fermion charge q_e is set to 1. (A) Γ/q_e as a function of m. Dotted line at $m/g = 0.3$ for reference. (B) Λ as a function of m. 80
4.6.1 Quantum quench protocol. 81

4.6.2 Plot of the Loschmidt echo density as a function of time for a quench from the free model to the interacting model. Blue line corresponds to $\mathcal{E}_0 = 0.0$. Yellow line corresponds to $\mathcal{E}_0 = 0.5$. . 85
4.6.3 Plot of the density of chiral condensate as a function of time for a quench from the free model to the interacting model. Blue line corresponds to $\mathcal{E}_0 = 0.0$. Yellow line corresponds to $\mathcal{E}_0 = 0.5$. . 86
4.6.4 Plot of the Loschmidt echo density as a function of time for a quantum quench between the massless interacting Hamiltonian with $\mathcal{E}_0 = 0.0$ to the massless interacting Hamiltonian with $\mathcal{E}_0 = 0.5$. 87
4.6.5 Plot of the order parameters as a function of time for a quantum quench between the massless interacting Hamiltonian with $\mathcal{E}_0 = 0.0$ to the massless interacting Hamiltonian with $\mathcal{E}_0 = 0.5$. (A) Axial fermion density. (B) Density of chiral condensate. 88

To my loved ones. I owe it all to you. Endure and transcend.

Acknowledgments

Foremost, I would first like to thank my thesis adviser professor Andrés Fernando Reyes. Prof. Reyes was always open to help whenever I had a question about this work. He always guided me towards the right path.

I would also like to thank all my teachers and mentors throughout all these years of studying physics. Special thanks to Pedro Bargueño, Alonso Botero and Andrés Flórez for all the time, dedication and teachings. Thank you for showing me the beauty and joy in physics.

I am grateful to all my friends in the office with whom the best moments were enjoyed and the worst moments were endured. The I-118 was a blast with you guys.

Finally, I would like to profoundly thank my parents and my girlfriend for their continuous and unconditional love, support and comprehension. Thank you for your patience and encouragement.

MRA, November 2018.

1

The continuum Schwinger model

1.1 Motivation and Introduction

Quantum electrodynamics in $1+1$ dimensions with massless fermions was a model first studied by Schwinger in 1962 [1] and thus it was coined the Schwinger model. This model is completely solvable using operator methods as demonstrated by Lowenstein and Swieca [2] and shows very interesting physical phenomena such as anomalies, a massive vector boson generated via a dynamical Higgs mechanism and the presence of confinement analogous to quark confinement in QCD_4 [3].

Hence, this model is a rich playground as a toy model for studying more complex gauge theories such as QCD_4 or supersymmetric gauge theories. Additionally, due to its simplicity, the Schwinger model is the perfect theory to first approach the subtleties in field theory such as anomalies, θ-vacua, bosonization, symmetry

breaking and non-perturbative methods in quantum field theory [3, 4].

In this chapter, we introduce the continuum Schwinger model and study its Lagrangian and its Hamiltonian. We derive the equations of motion that give rise to the dynamics of the system. Special emphasis is made on the fact that the model simplifies greatly over its cousin QED_4 due to the simplicity of electrodynamics in $D = 2$. We derive using only the equations of motion that this model has a massive electromagnetic Boson, with its mass being proportional to the electromagnetic coupling constant q_e. We also discuss the energetics of pair production in one spatial dimension, and how this gives rise to a background electric field which induces a critical behavior in the system. Such behavior is a consequence of a discontinuity in the vacuum energy density due to the background field.

Secondly, we explore the chiral anomaly of the model and derive its exact value using the path integral formalism. The anomaly appears as a consequence of the classical action having two symmetries, a gauge $U(1)$ symmetry and an axial $U_A(1)$ symmetry, which upon quantization come into conflict yielding an anomalous divergence of the Noether current associated to the $U_A(1)$. Furthermore, we comment how this anomaly is directly related to the topology of the theory and can be understood by invoking the Atiyah-Singer index theorem relating the index of the Dirac operator and the topological information of the $U(1)$ gauge group.

Finally, we explore how the anomaly presents itself as a non-trivial restructuring of the fermion energy levels and the effect this restructuring has on the physical spectrum of the theory and the conserved charges associated to the symmetries of the model. Moreover, we study how the anomaly can be understood as both an infrared and an ultraviolet phenomenon, which originates from the fermion levels crossing the vacuum energy level and the ultraviolet cutoff correspondingly.

1.2 Lagrangian, Hamiltonian and equations of motion

As a first step let us study the Lagrangian of QED_4, the close cousin of the Schwinger model. The Lagrangian reads

$$\mathscr{L} = \bar{\psi}(i\partial\!\!\!/ - m)\psi - \frac{1}{4}F_{\mu\nu}^2 - q_e\bar{\psi}A\!\!\!/\psi. \tag{1.1}$$

In $3+1$ dimensions the coupling constant is dimensionless having th value $q_e^2 = 4\pi/137$. In units in which $\hbar = c = 1$ we have

$$[M] = [L]^{-1} = [T]^{-1}. \tag{1.2}$$

Thus we have that the action $S = \int \mathrm{d}^2x\,\mathscr{L}$ is dimensionless which implies

$$[\mathscr{L}] = [M]^2.$$

The free Dirac Lagrangian $\mathscr{L}_{\text{Dirac}} = \bar{\psi}(i\partial\!\!\!/ - m)\psi$ implies that

$$[\bar{\psi}\psi] = [M].$$

Also, the free Maxwell Lagrangian must satisfy

$$[F_{\mu\nu}^2] = [(\partial_\mu A_\nu - \partial_\nu A_\mu)^2] = [M]^2,$$

which implies

$$[A_\mu] = [M]^0.$$

Hence, the interaction Lagrangian must have dimensions

$$\mathscr{L}_{\text{int}} = -q_e\bar{\psi}A\!\!\!/\psi = [M]^2.$$

The previous dimensional analysis yields

$$[M]^2 = [q_e][M] \Rightarrow [q_e] = [M].$$

In a later section, we will prove that the axial anomaly creates a mass-generating mechanism for the gauge vector Boson (the "photon") which in this model has a mass $m_\gamma^2 = q_e^2/\pi$. Thus in this theory, the Boson carrying the electromagnetic interaction has a mass which is proportional to the interaction coupling constant.

After this short detour, we can focus our attention on the Lagrangian for the Schwinger model

$$\mathscr{L} = \bar{\psi}(i\not{D})\psi - \frac{1}{4}F_{\mu\nu}^2, \tag{1.3}$$

with the covariant derivative $D_\mu = \partial_\mu + iq_e A_\mu$. In 1+1 dimensional Minkowski space the metric $g_{\mu\nu}$ $(\mu, \nu = 0, 1)$ is

$$g = \begin{pmatrix} 1 & 0 \\ 0 & -1 \end{pmatrix}. \tag{1.4}$$

The Dirac matrices fulfill

$$\{\gamma^\mu, \gamma^\nu\} = 2g^{\mu\nu} \tag{1.5}$$

which implies that

$$(\gamma^0)^2 = 1$$

$$(\gamma^1)^2 = -1$$

and

$$\{\gamma^0, \gamma^1\} = 0.$$

Therefore we can choose one of the following representations for the gamma matrices

$$\gamma^0 = \sigma^1, \qquad \gamma^1 = -i\sigma^2, \qquad \gamma_5 = \gamma^0\gamma^1 = \sigma^3, \tag{1.6}$$

or

$$\gamma^0 = \sigma^3, \qquad \gamma^1 = -i\sigma^2, \qquad \gamma_5 = \gamma^0\gamma^1 = \sigma^1. \tag{1.7}$$

Both this representations imply that

$$(\gamma_5)^2 = 1$$

and

$$\{\gamma_5, \gamma^\mu\} = 0.$$

Let us now turn our attention towards the Lagrangian of the theory (1.3)

$$\mathscr{L} = \bar{\psi}(i\partial\!\!\!/)\psi - \frac{1}{4}\left(\partial_\mu A_\nu - \partial_\nu A_\mu\right)^2 - q_e\bar{\psi}\gamma^\nu\psi A_\nu$$

To obtain the equations of motion for the theory we employ the Euler-Lagrange equations

$$\partial_\mu \frac{\partial\mathscr{L}}{\partial(\partial_\mu\psi)} = \frac{\partial\mathscr{L}}{\partial\psi}. \tag{1.8}$$

which yield the Dirac equation

$$(iD\!\!\!/ - m)\psi = 0, \tag{1.9}$$

and

$$\partial_\mu \frac{\partial\mathscr{L}}{\partial(\partial_\mu A_\nu)} = \frac{\partial\mathscr{L}}{\partial A_\nu}, \tag{1.10}$$

yielding Maxwell's equations

$$\partial_\mu F^{\nu\mu} = -q_e\bar{\psi}\gamma^\nu\psi \doteq -q_e J^\nu.$$

Hence, as in standard QED_4 we get

$$\partial_\mu F^{\mu\nu} = q_e J^\nu. \tag{1.11}$$

We can take the divergence of (1.11) and using the fact that $F^{\mu\nu}$ is anti-symmetric we obtain the usual current conservation law

$$\partial_\nu \partial_\mu F^{\mu\nu} = 0 = q_e \, \partial_\nu J^\nu. \tag{1.12}$$

Let us also introduce the anti-symmetric tensor $\varepsilon_{\mu\nu}$ defined by $\varepsilon_{01} = -\varepsilon_{10} = 1$. The following relation is easily proved

$$\varepsilon^{\mu\nu} = g^{\mu\rho}\varepsilon_{\rho\sigma}g^{\sigma\nu} = \begin{pmatrix} 0 & -1 \\ 1 & 0 \end{pmatrix} = -\varepsilon_{\mu\nu}.$$

Using this result we can prove the following very important relationship for the gamma matrices in two dimensions:

$$\gamma^\mu \gamma_5 = \varepsilon^{\mu\nu}\gamma_\nu \tag{1.13}$$

$$\gamma^\mu\gamma_5 = \gamma^\mu\gamma^0\gamma^1 = \begin{cases} (\gamma^0)^2\gamma^1 = \gamma^1 = -\gamma_1 = \varepsilon^{01}\gamma_1 = \varepsilon^{0\nu}\gamma_\nu & \text{for } \mu = 0 \\ \gamma^1\gamma^0\gamma^1 = -\gamma^0(\gamma^1)^2 = \gamma^0 = \gamma_0 = \varepsilon^{10}\gamma_0 = \varepsilon^{1\nu}\gamma_\nu & \text{for } \mu = 1. \end{cases}$$

The relation (1.13) allows expressing the axial current as the dual of the current vector

$$J^\mu_5 \doteq \bar\psi\gamma^\mu\gamma_5\psi = \varepsilon^{\mu\nu}\bar\psi\gamma^\mu\psi = \varepsilon^{\mu\nu}J_\nu \doteq {}^*J^\mu. \tag{1.14}$$

Now, to write the equations of motion for the dual field strength tensor and the dual current we can use the following identity:

$$F_{\mu\nu} = \varepsilon_{\mu\nu}F_{01}, \tag{1.15}$$

since $F_{00} = F_{11} = 0$ and $F_{01} = \varepsilon_{01}F_{01} = \varepsilon_{10}F_{10}$. Thus, the dual to the F-tensor

is the following scalar

$$^*F = \frac{1}{2}\varepsilon^{\mu\nu}F_{\mu\nu} = \frac{1}{2}\varepsilon^{\mu\nu}\varepsilon_{\mu\nu}F_{01} = -F_{01}, \tag{1.16}$$

here we have used the fact that $\varepsilon^{\mu\nu}\varepsilon_{\mu\nu} = -\delta^{\mu}_{\mu} = -2$. This immediately tells us that

$$F_{\mu\nu} = -\varepsilon_{\mu\nu}{}^*F, \tag{1.17}$$

consequently, this leads to a dual equation of motion for $^*F$, viz

$$\partial_\mu {}^*F = -q_e J^5_\mu. \tag{1.18}$$

In the following section, we will show that by using the anomalous divergence of the axial current due to the chiral anomaly we get the following equation

$$\left(\Box + \frac{q_e^2}{\pi}\right){}^*F = 0. \tag{1.19}$$

Hence, as suggested at the beginning of the chapter, even at the level of the equations of motion we can see the appearance of a massive gauge Boson, the photon, whose mass is $m_\gamma = e/\sqrt{\pi}$.

Let us now study the Hamiltonian of the Schwinger model. We can compute the Hamiltonian by first obtaining the canonical energy-momentum tensor as the conserved Noether current of spacetime translations, viz

$$T^\mu{}_\nu = \frac{\partial \mathscr{L}}{\partial(\partial_\mu \psi)}\partial_\nu \psi + \text{c.c} - \delta^\mu{}_\nu \mathscr{L}. \tag{1.20}$$

Since the Lagrangian (1.3) only depends on $\partial_\mu\psi$ equation (1.20) yields the following energy-momentum tensor

$$T^{\mu\nu} = i\bar{\psi}\gamma^\mu\partial^\nu\psi - g^{\mu\nu}\mathscr{L}. \tag{1.21}$$

We can use the equations of motion to set $\mathscr{L} = 0$, obtaining

$$T^{\mu\nu} = i\bar{\psi}\gamma^{\mu}\partial^{\nu}\psi. \tag{1.22}$$

We can find the total energy of the field as

$$H = \int d^2x\, T^{00} = \int d^2x\, i\bar{\psi}\gamma^0\partial^0\psi = \int d^2x\, \bar{\psi}(-i\gamma^1\partial^1 + m)\psi, \tag{1.23}$$

to obtain the last equality we have made use of the equations of motion and we have added a mass term for the sake of completeness.

The previous derivation of the Hamiltonian and the total energy of the field is all concerning the Dirac field. However, we are interested in the full energy-momentum tensor for the Schwinger model. This tensor is simply obtained by adding the energy density of the Electric field in $(1+1)$-dimensional space and replacing derivatives ∂ with covariant derivatives D. Furthermore, we can fix a gauge in which $A_0 = 0$, the field tensor becomes $F_{01} = -\partial_0 A_1 = E$ and with this the Hamiltonian is written as

$$H = \int d^2x \left(-i\bar{\psi}\gamma^1(\partial_1 + iq_e A_1)\psi + m\bar{\psi}\psi + \frac{1}{2}E^2\right). \tag{1.24}$$

1.2.1 The Schwinger model in a Background electric field

If we fix a gauge such that $A_0 = 0$ Maxwell's equations (1.11) reduce to single equation

$$\partial_x E = q_e J^0 \tag{1.25}$$

which is Gauss's law. Since we are working in 1 spatial dimension it is easy to

integrate (1.25)

$$E = q_e \int \mathrm{d}x J^0(x) + \mathcal{E}, \tag{1.26}$$

where $\mathcal{E}$ is a constant background field which we can imagine as being generated by a parallel plate capacitor at both ends of the one-dimensional universe. This background field induces a very interesting physical behavior that was first described by Sydney Coleman in a beautiful paper [5]. Coleman explains that we can analyze the effect of this background field by considering a particle-antiparticle pair separated by a distance x as seen in figure 1.2.1.

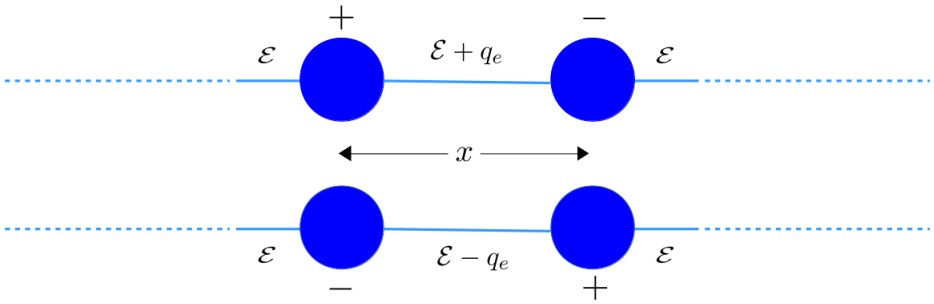

Figure 1.2.1: Two distinct configurations for particle-antiparticle pairs in one spatial dimension.

The energy difference of this configuration compared to a vacuum state with no particles or antiparticles is given by

$$\Delta E = \frac{1}{2} \int \mathrm{d}x \left[(F_{01}) - \mathcal{E} \right] = \frac{x}{2} [(\mathcal{E} \pm q_e)^2 - \mathcal{E}^2]. \tag{1.27}$$

In essence, we can understand (1.27) as saying that it is energetically disfavorable for the vacuum to induce pair production if $|\mathcal{E}| \leq q_e/2$. However, if $|\mathcal{E}| > q_e/2$ the pair production from vacuum will set in and charges will travel to opposite edges of the spatial dimension until the field strength $\mathcal{E}$ is lowered below $q_e/2$. This implies that the physics is periodic in $\mathcal{E}$ with period q_e.

Furthermore, we can define a dimensionless quantity

$$\mathcal{E}_0 \doteq \frac{\mathcal{E}}{q_e}$$

such that $\mathcal{E}_0 \in [0, 1]$. In the weak coupling limit $m/q_e \to \infty$, there is no particle-antiparticle pairs present and the vacuum energy density ε is due to the electrostatic energy only since we can renormalize the Dirac sea energy of fermions to 0. Thus we have that in this limit

$$\varepsilon = \begin{cases} \dfrac{\mathcal{E}^2}{2} = \dfrac{q_e^2 \mathcal{E}_0^2}{2} & \text{if } \mathcal{E}_0 \leq \dfrac{1}{2} \\ \dfrac{(q_e - \mathcal{E})^2}{2} = \dfrac{q_e^2}{2}(1 - \mathcal{E}_0)^2 & \text{if } \mathcal{E}_0 > \dfrac{1}{2}. \end{cases} \tag{1.28}$$

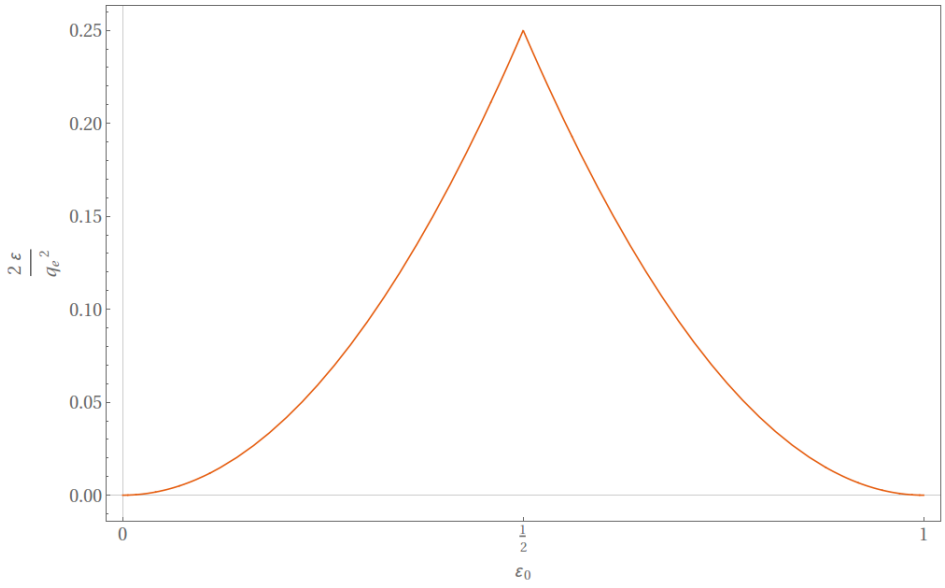

Figure 1.2.2: Plot of energy density as a function of $\mathcal{E}_0$.

This is shown in figure 1.2.2. As we can see from figure 1.2.2, ε has a sharp peak at $\mathcal{E}_0 = 1/2$, which points to the existence of a first order phase transition.

1.3 Chiral anomaly in the path integral formalism

1.3.1 Path integrals and the Grassman Jacobian

Let us discuss the subtleties and important features of the Schwinger model that are closely related to the anomaly. Since the functional and path integral techniques are better suited to Euclidean space we will perform a Wick rotation $x_0 = -ix_4$ to arrive at Euclidean space with a negative metric $g_{\mu\nu} = -\delta_{\mu\nu}$. In Euclidean space we have that:

$$\partial_0 = i\partial_4, \quad A_0 = iA_4, \quad D_0 = iD_4, \quad \gamma^4 = i\gamma^0, \quad \gamma_5 = \gamma^0\gamma^1 = i\gamma^1\gamma^4.$$

With this convention we have the following important relations in Euclidean space ($\mu = 4, 1$):

$$(\gamma^\mu)^\dagger = -\gamma^\mu \tag{1.29}$$

$$(\gamma^\mu)^2 = -1 \tag{1.30}$$

and

$$(\gamma_5)^2 = 1. \tag{1.31}$$

Here the Dirac operator is Hermitian, $\not{D}^\dagger = \not{D}$ and $\varepsilon_{41} = i\varepsilon_{10}$. The following relations for the gamma matrices also hold in Euclidean space and will be useful throughout

$$\gamma_\mu\gamma_5 = \varepsilon_{\mu\nu}\gamma^\nu \tag{1.32}$$

$$[\gamma^\mu, \gamma^\nu] = -2\varepsilon^{\mu\nu}\gamma_5 \tag{1.33}$$

$$\mathrm{Tr}(\gamma^\mu\gamma^\nu) = \frac{1}{2}\,\mathrm{Tr}([\gamma^\mu,\gamma^\nu] + \{\gamma^\mu,\gamma^\nu\}) = -2\delta^{\mu\nu} \tag{1.34}$$

$$\mathrm{Tr}\big(\gamma_5\gamma^\mu\gamma^\nu\big) = 2i\varepsilon^{\mu\nu}. \tag{1.35}$$

After this short detour on useful relations, let us explore the origin of the axial vector anomaly as a consequence of a change in the measure of the fermionic path integral. We start with the generating functional of a massless fermion ψ coupled to electrodynamics in 2 dimensions

$$\mathcal{Z} = \int \mathcal{D}A_\mu \mathcal{D}\psi\mathcal{D}\bar{\psi} e^{S[A,\psi,\bar{\psi}]} \tag{1.36}$$

with the classical action

$$S = \int \mathrm{d}^2x \left(\bar{\psi}(i\not{D})\psi - \frac{1}{4}F_{\mu\nu}^2\right). \tag{1.37}$$

This theory has a $U_A(1)$ axial or chiral symmetry

$$\begin{aligned} \psi &\to e^{i\beta(x)\gamma_5}\psi = \psi + i\beta(x)\gamma_5\psi \\ \bar{\psi} &\to \bar{\psi}e^{i\beta(x)\gamma_5} = \bar{\psi} + i\bar{\psi}\beta(x)\gamma_5 \end{aligned} \tag{1.38}$$

with a corresponding Noether current J_5^μ for this symmetry. In quantum field theory, the classical Noether conservation law is replaced by the existence of Ward identities. To explore this we need to study the effect of the infinitesimal chiral transformation to the Grassmann integration measure $\mathcal{D}\psi\mathcal{D}\bar{\psi}$. First, we need to compute the functional Jacobian defined by

$$\mathcal{D}\psi\mathcal{D}\bar{\psi} \to \mathcal{D}\psi'\mathcal{D}\bar{\psi}' = J[\beta]\mathcal{D}\psi\mathcal{D}\bar{\psi}. \tag{1.39}$$

To first order in β the fermionic Lagrangian changes like

$$\begin{aligned}\bar{\psi}'(i\not{D})\psi' &= (\psi + i\beta(x)\gamma_5\psi)i\not{D}(\bar{\psi} + i\bar{\psi}\beta(x)\gamma_5)\\ &= \bar{\psi}(i\not{D})\psi - [\partial_\mu\beta(x)]\bar{\psi}\gamma^\mu\gamma_5\psi + \mathcal{O}(\beta^2). \qquad (1.40)\end{aligned}$$

Therefore the fermionic part of the generating functional is transformed as follows

$$\begin{aligned}&\int \mathcal{D}\psi'\mathcal{D}\bar{\psi}' \exp\left(\int \mathrm{d}^2x\, \bar{\psi}'(i\not{D})\psi\right)\\ &\to J[\beta]\int \mathcal{D}\psi\mathcal{D}\bar{\psi}\exp\left(\int \mathrm{d}^2x\, \bar{\psi}(i\not{D} - \partial_\mu\beta(x)\gamma^\mu\gamma_5)\psi\right) \qquad (1.41)\end{aligned}$$

where both sides of (1.41) are Gaussian Grassmann integrals. These Gaussian integrals of Grassmann variables are equal to

$$\det(i\not{D}) = J[\beta]\det\big(i\not{D} - \partial_\mu\beta(x)\gamma^\mu\gamma_5\big), \qquad (1.42)$$

thus the value of the Jacobian $J[\beta]$ is given as the ratio of two determinants.

Now, we need to expand the spinors in terms of eigenfunctions of the Dirac operator

$$i\not{D}\varphi_n \equiv i(\not{\partial} + ie\not{A})\varphi_n = \lambda_n\varphi_n, \qquad (1.43)$$

having the completeness relation given by the inner product

$$\int \mathrm{d}^2x\, \varphi_n^\dagger(x)\varphi_m(x) = \delta_{nm}. \qquad (1.44)$$

Thus, on this basis the spinors are decomposed as

$$\psi = \sum_n a_n\varphi_n; \quad \bar{\psi} = \sum_n b_n\varphi_n^\dagger, \qquad (1.45)$$

where the coefficients a_n and $\bar{b}_n$ are independent elements of the Grassmann

algebra. The fermionic measure is then defined to be

$$\mathcal{D}\psi\mathcal{D}\bar{\psi} \doteq \prod_n \mathrm{d}b_n \mathrm{d}a_n. \tag{1.46}$$

Under a chiral transformation (1.38) the Grassmann coefficients in (1.45) are transformed to

$$\psi = \sum_n a'_n \varphi_n = \sum_n a_n e^{i\beta(x)\gamma_5} \varphi_n \tag{1.47}$$

which implies that infinitesimally

$$\begin{aligned} a'_n &= \sum_n \int \mathrm{d}^2x\, \varphi^\dagger_m(x)(1 + i\beta(x)\gamma_5 + \ldots)\varphi_n(x) a_n \\ &= \sum_n (\delta_{nm} + \mathbb{A}_{nm}) a_n. \end{aligned} \tag{1.48}$$

Therefore, the measure is transformed as

$$\prod_n \mathrm{d}a'_n = [\det(1 + \mathbb{A}_{nm})]^{-1} \prod_n \mathrm{d}a_n, \tag{1.49}$$

the inverse power of the determinant is a consequence of the translation invariance of the Grassmann integration measure and the fact that Grassmann integration is the same as usual differentiation with the equivalence given by

$$\mathrm{d}a_n \equiv \partial/\partial a_n \,.$$

The Jacobian for $\mathcal{D}\bar{\psi}$ gives rise to an identical factor as (1.49). Consequently, we have that

$$\prod_n \mathrm{d}b_n \mathrm{d}a_n. = [\det(1 + \mathbb{A}_{nm})]^{-2} \prod_n \mathrm{d}b_n \mathrm{d}a_n, \tag{1.50}$$

Thus, we need to compute

$$\det\left(1+\mathbb{A}_{nm}\right)=\exp\left(\operatorname{tr}\log(1+\mathbb{A}_{nm})\right),$$

which to first order in β is simply $\exp(\operatorname{tr}\mathbb{A}_{nm})$. Hence,

$$J[\beta]=\left[\det\left(1+\mathbb{A}_{nm}\right)\right]^{-2}=\exp\left(-2i\int \mathrm{d}^2x\,\beta(x)\sum_n \varphi_n^\dagger(x)\gamma_5\varphi_n(x)\right). \quad (1.51)$$

1.3.2 Dirac operator mode regularization

The coefficient of $\beta(x)$ is $\operatorname{tr}\gamma_5$ which is zero. However, the trace is also over an infinite number of eigenstates of $i\not{D}$, which of course is infinite. Consequently, (1.51) is an ill-defined sum which should be regularized in order to obtain a sensible result. We can regulate (1.51) by introducing a UV-regulator to cut off the sum at large eigenvalues

$$\sum_n \varphi_n^\dagger(x)\gamma_5\varphi_n(x)\equiv\lim_{M\to\infty}\sum_n \varphi_n^\dagger(x)\gamma_5\varphi_n(x)e^{\lambda_n/M^2}. \quad (1.52)$$

Since the φ_n are eigenfucntions of $i\not{D}$ we can introduce the one-particle Hilbert space $\{|x\rangle\}$ and write (1.52) equivalently as

$$\lim_{M\to\infty}\sum_n \varphi_n^\dagger(x)\gamma_5 e^{(i\not{D})^2/M^2}\varphi_n(x)=\lim_{M\to\infty}\left\langle x\middle|\operatorname{tr}\left(\gamma_5 e^{(i\not{D})^2/M^2}\right)\middle|x\right\rangle. \quad (1.53)$$

This being so, we need to find an expression for $-\not{D}^2$ in terms of the gauge field A_μ. This is done as follows, consider the Dirac equation

$$i(\not{\partial}+iq_e\not{A})\psi=0, \quad (1.54)$$

since it is equated to zero we can multiply it by whatever we want. An intelligent choice is to multiply by

$$
\begin{aligned}
0 &= (i\not{\partial} - q_e\not{A})(i\not{\partial} - q_e\not{A})\psi \\
&= \left(\frac{1}{4}\left\{i\partial_\mu - q_eA_\mu, i\partial_\nu - q_eA_\nu\right\}\{\gamma^\mu, \gamma^\nu\} + \left[i\partial_\mu - q_eA_\mu, i\partial_\nu - q_eA_\nu\right][\gamma^\mu, \gamma^\nu]\right)\psi \\
&= \left[(i\partial_\mu - q_eA_\mu)(i\partial_\nu - q_eA_\nu)g^{\mu\nu} + \frac{iq_e}{2}F_{\mu\nu}\varepsilon^{\mu\nu}\gamma_5\right]\psi \\
&= \left[(i\partial_\mu - q_eA_\mu)^2 + \frac{iq_e}{2}F_{\mu\nu}\varepsilon^{\mu\nu}\gamma_5\right]\psi. \qquad (1.55)
\end{aligned}
$$

We recognize the expression inside brackets as $\not{D}^2 = D^2 + \frac{iq_e}{2}F_{\mu\nu}\varepsilon^{\mu\nu}\gamma_5$.
Moreover, we need to evaluate

$$
\lim_{M\to\infty}\beta(x)\left\langle x\middle|\mathrm{tr}\left(\gamma_5\exp\left(-\frac{(\partial - q_eA)^2 + \frac{iq_e}{2}F_{\mu\nu}\varepsilon^{\mu\nu}\gamma_5}{M^2}\right)\right)\middle|x\right\rangle \qquad (1.56)
$$

Expanding the exponential to extract the contribution to leading e we get that

$$
\lim_{M\to\infty}\beta(x)\left\langle x\middle|\mathrm{tr}\left(\gamma_5\exp\left(-\frac{(\partial - q_eA)^2}{M^2}\right)\left(1 - \frac{iq_e}{2}F_{\mu\nu}\varepsilon^{\mu\nu}\gamma_5\right)\right)\middle|x\right\rangle. \qquad (1.57)
$$

Here we can set $A = 0$ obtaining

$$
\begin{aligned}
&\lim_{M\to\infty}\beta(x)\left\langle x\middle|\mathrm{tr}\left(\gamma_5 e^{-\frac{\partial^2}{M^2}}\left(1 - \frac{iq_e}{2}F_{\mu\nu}\varepsilon^{\mu\nu}\gamma_5\right)\right)\middle|x\right\rangle \\
&= \lim_{M\to\infty}\beta(x)\left(\frac{-iq_e}{2M^2}F_{\mu\nu}\varepsilon^{\mu\nu}\right)\mathrm{tr}\left[(\gamma_5)^2\right]\left\langle x\middle|e^{-\frac{\partial^2}{M^2}}\middle|x\right\rangle. \qquad (1.58)
\end{aligned}
$$

Using the fact that

$$
\left\langle x\middle|e^{-\frac{\partial^2}{M^2}}\middle|x\right\rangle = i\int\frac{\mathrm{d}^2k_E}{(2\pi)^2}e^{-k_E/M^2} = \frac{iM^2}{2\pi}, \qquad (1.59)
$$

where the subscript E refers to Euclidean momenta. We have that the contribution to leading order in e is independent of M. Hence, when the regulator mass $M \to \infty$ we obtain

$$\frac{q_e}{4\pi} F_{\mu\nu}\varepsilon^{\mu\nu}. \tag{1.60}$$

which is the 2 dimensional version of the Adler–Bell–Jackiw anomaly [6, 7].

Hence, the evaluation of the Jacobian $J[\beta]$ in (1.51) is

$$J[\beta] = \exp\left(i \int \mathrm{d}^2x\, \beta(x) \frac{q_e}{2\pi} F_{\mu\nu}\varepsilon^{\mu\nu}\right). \tag{1.61}$$

The result of a chiral transformation to the fermionic measure is then

$$\begin{aligned} &\int \mathcal{D}\psi\mathcal{D}\bar{\psi} \exp\left(\int \mathrm{d}^2x\, \mathscr{L}_{\mathrm{QED}_2}\right) \\ &\quad \to \int \mathcal{D}\psi\mathcal{D}\bar{\psi} \exp\left(\int \mathrm{d}^2x\, \mathscr{L}_{\mathrm{QED}_2} - J^5_\mu \partial_\mu \beta(x) + i\beta(x) \frac{q_e}{2\pi} F_{\mu\nu}\varepsilon^{\mu\nu}\right) \end{aligned} \tag{1.62}$$

1.3.3 Schwinger-Dyson equation for a gauge symmetry

In classical field theory, Noether's theorem stems from the fact that a variation of the field being a global symmetry of the Lagrangian leads to the existence of a classical conserved Noether current. The quantum field theory counterpart of this procedure, in the path integral formalism, will produce a powerful result concerning the correlation functions the theory. To derive the result let us consider the correlation function of $\psi(x_1)$ and $\bar{\psi}(x_2)$ in a fermionic theory with a *global symmetry*

$$\psi \to e^{i\alpha}\psi,$$

this correlator reads

$$\langle \psi(x_1)\bar{\psi}(x_2)\rangle = \int \mathcal{D}\psi\mathcal{D}\bar{\psi}\exp\left(\int \mathrm{d}^2x\,\bar{\psi}(i\partial\!\!\!/ + m)\psi\right)\psi(x_1)\bar{\psi}(x_2). \tag{1.63}$$

The field transform locally as

$$\psi(x) \to e^{-ia(x)}\psi(x); \quad \bar{\psi}(x) \to e^{ia(x)}\bar{\psi}(x) \tag{1.64}$$

Therefore, under this transformation, the Lagrangian is not invariant, as it acquires the following terms

$$i\bar{\psi}\partial\!\!\!/\psi \to i\bar{\psi}\partial\!\!\!/\psi + \bar{\psi}\gamma^\mu\psi\partial_\mu a(x), \tag{1.65}$$

and

$$\psi(x_1)\bar{\psi}(x_2) \to e^{-ia(x_1)}e^{ia(x_2)}\psi(x_1)\bar{\psi}(x_2) \tag{1.66}$$

The path integral is invariant under *any* field redefinition up to a Jacobian factor, $J[a]$, which in the case of a transformation like (1.64) is equal to 1. Hence, expanding to first order in a leads to the following relation

$$\begin{aligned} 0 = &\int \mathcal{D}\psi\mathcal{D}\bar{\psi}e^{iS[\psi,\bar{\psi}]}\left(i\int \mathrm{d}^2x\,\bar{\psi}\gamma^\mu\psi\partial_\mu a(x)\right)\psi(x_1)\bar{\psi}(x_2) \\ &+ \int \mathcal{D}\psi\mathcal{D}\bar{\psi}e^{iS[\psi,\bar{\psi}]}(-ia(x_1)\psi(x_1)\bar{\psi}(x_2) + ia(x_2)\psi(x_1)\bar{\psi}(x_2)). \end{aligned} \tag{1.67}$$

A simple and clever rearrangement of the previous relation yields the following very important result:

$$\int \mathrm{d}^2x\, i\alpha(x)\partial_\mu \int \mathcal{D}\psi\mathcal{D}\bar{\psi} e^{iS[\psi,\bar{\psi}]}(\bar{\psi}\gamma^\mu\psi)\psi(x_1)\bar{\psi}(x_2)$$
$$= \int \mathrm{d}^2x\, i\alpha(x)(\delta(x-x_2)-\delta(x-x_1)) \int \mathcal{D}\psi\mathcal{D}\bar{\psi} e^{iS[\psi,\bar{\psi}]}\psi(x_1)\bar{\psi}(x_2). \quad (1.68)$$

Since this must hold for arbitrary α, we have the following relation for the correlation functions

$$\partial_\mu \langle J^\mu \psi(x_1)\bar{\psi}(x_2)\rangle = -\delta(x-x_1)\langle \psi(x_1)\bar{\psi}(x_2)\rangle + \delta(x-x_2)\langle \psi(x_1)\bar{\psi}(x_2)\rangle \quad (1.69)$$

where we have recalled the definition of the $\mathrm{U}(1)$ electromagnetic current $J^\mu \doteq \bar{\psi}\gamma^\mu\psi$. This relation is the quantum conservation law analogous to the classical $\partial_\mu J^\mu = 0$ and holds for time-ordered correlation functions in quantum field theory. Moreover, the relation is easily generalized to higher order correlation functions. It contains one delta function for each spinor field ψ_i of charge Q_i in the correlation function [8], namely

$$\partial_\mu \langle J^\mu \psi(x_1)\bar{\psi}(x_2)A^\nu(x_3)\bar{\psi}(x_4)+\cdots\rangle = \sum Q_i\delta(x-x_i)\langle \psi(x_1)\bar{\psi}(x_2)A^\nu(x_3)\bar{\psi}(x_4)+\cdots\rangle \quad (1.70)$$

This equation is independent of gauge fixing and thus neither the photon field A^ν nor the photon kinetic term $F^{\mu\nu}$ have any effect in the final expression for the correlation function.

Hence, in the case of (1.62) the proper relation for the correlator function reads

$$\partial_\mu \left\langle J^\mu_5 \mathcal{O}(x_1\ldots x_n)\right\rangle = [i]\frac{q_e}{2\pi}\left\langle \varepsilon^{\mu\nu}F_{\mu\nu}\mathcal{O}(x_1\ldots x_n)\right\rangle \quad (1.71)$$

for any local operator $\mathcal{O}(x_1\ldots x_n)$. It is important to note that the factor i in

brackets in front of the result is absent in Minkowski space. In such a way and after a rather long calculation, we have found that the anomalous divergence of the axial current in the Schwinger model which is given by (1.71).

1.4 Anomaly, index and topology

1.4.1 Zero-modes and index of the Dirac operator

Fujikawa realized that the exponential in the transformation of the Jacobian $J[\beta]$ represents an *"index density"* of the Dirac operator [9]. To see this let us introduce the following projectors

$$P_{\pm} = \frac{1 \pm \gamma_5}{2}, \tag{1.72}$$

such that

$$P_{\pm}\psi = \psi_{\pm}; \quad \gamma_5\psi_{\pm} = \pm\psi_{\pm}, \tag{1.73}$$

with the positive and negative chirality spinors

$$\psi_{-} = \begin{pmatrix} \psi_1 \\ 0 \end{pmatrix}, \quad \psi_{+} = \begin{pmatrix} 0 \\ \psi_2 \end{pmatrix}. \tag{1.74}$$

Let us recall that we can expand the Dirac operator in eigenmodes:

$$i\not{D}\psi_n = \lambda_n\psi_n, \tag{1.75}$$

since $\{\gamma^\mu, \gamma_5\} = 0$, $\gamma_5\psi_n$ satisfies the following eigenvalue equation

$$i\not{D}\gamma_5\psi_n = -\lambda_n\gamma_5\psi_n. \tag{1.76}$$

Now, given the inner product in Euclidean space and using the fact that $i\not{D}$ is

Hermitian, for $\lambda_n \neq 0$ we have hat both eigenfunctions are orthogonal, viz

$$\left\langle \psi_n \middle| \gamma_5 \psi_n \right\rangle = \int \mathrm{d}^2x \, \psi_n^*(x) \gamma_5 \psi_n(x) = 0. \tag{1.77}$$

Nonetheless, for $\lambda_n = 0$, we can define *zero-modes* Φ_n which satisfy

$$i\not{D}\Phi_n = 0; \quad i\not{D}\gamma_5\Phi_n = 0, \tag{1.78}$$

being simultaneously eigenfunctions of γ_5 for positive and negative chirality spinors

$$\gamma_5\Phi_n^+ = +\Phi_n^+; \quad \gamma_5\Phi_n^- = +\Phi_n^-. \tag{1.79}$$

Recalling the transformation of the Jacobian $J[\beta]$ in terms of the eigenmodes of the Dirac operator (1.51), we obtain, in terms of the zero-modes

$$\begin{aligned} \int \mathrm{d}^2x \sum_n \psi_n^* \gamma_5 \psi_n &= \int \mathrm{d}^2x \sum_{\substack{n \\ \lambda_n = 0}} \Phi_n^{+*} \gamma_5 \Phi_n \\ &= \sum_{\substack{n \\ \lambda_n = 0}} \int \mathrm{d}^2x \, \Phi_n^{+*} \Phi_n^+ - \sum_{\substack{n \\ \lambda_n = 0}} \int \mathrm{d}^2x \, \Phi_n^{-*} \Phi_n^- \equiv (n_+ - n_-). \end{aligned} \tag{1.80}$$

Here we see the appearance of the number of zero-modes of positive and negative chirality, respectively n_+ and n_-. The difference in equation (1.80) is known as the *index* of a differential operator. The differential operator we are considering is

$$D_+ \equiv i\not{D}P_+ \tag{1.81}$$

with the adjoint operator given by

$$D_+^\dagger = D_- \equiv i\not{D}P_-. \tag{1.82}$$

These operators act on the subspaces of positive and negative chirality respectively.

Now, the index of a Fredholm operator such as D_+ is defined as

$$\mathrm{ind}D_+ = \dim(\ker D_+) - \dim(\mathrm{coker}D_+) = \dim(\ker D_+) - \dim(\ker D_+^\dagger), \tag{1.83}$$

but the difference in (1.83) is precisely $n_+ - n_-$, the difference between the number of positive and negative chirality zero-modes.

To make a connection to the anomaly computation done in section 1.3 let us recall that in order to make sense of the Jacobian $J[\beta]$, we had to include an UV-regulator. This regulator allowed us to compute the sum in equation (1.80) in terms of the gauge field strength tensor. Combining (1.80) and (1.52) yields

$$\frac{q_e}{4\pi}\int \mathrm{d}^2x\, \varepsilon_{\mu\nu}F^{\mu\nu} = (n_+ - n_-) \equiv \mathrm{ind}D_+. \tag{1.84}$$

This result is the *Atiyah-Singer theorem* for the Dirac operator coupled to a $U(1)$ gauge field in two-dimensional Euclidean space.

1.4.2 Atiyah-Singer index theorem

Atiyah and Singer [10] showed that the index of an elliptic differential operator can be expressed in terms of purely topological quantities. In the case of the Dirac operator coupled to a Yang-Mills field in even-dimensional space their result is

$$\mathrm{ind}D_+ = \int_{\mathcal{M}} \mathrm{ch}F \tag{1.85}$$

where ch is the Chern character and $\mathcal{M}$ is a compact $2n$-dimensional manifold equipped with a spin connection ω. The Chern class is given by

$$\mathrm{ch}F = \mathrm{tr}\, e^{\frac{i}{2\pi}F} = \boldsymbol{r} + \frac{1}{2\pi}\mathrm{tr}\, F + \frac{1}{2!}\left(\frac{i}{2\pi}\right)\mathrm{tr}\, F^2 + \dots \tag{1.86}$$

for a representation $\boldsymbol{r}$ of a $SU(N)$ (or $U(N)$) gauge connection A, with curvature 2-form $F = \mathrm{d}A + A^2$. Since the integral is done over $\mathcal{M}$ only the n-th term in (1.86)

survives. Moreover since all physical quantities vanish at infinity, in particular $J^5_\mu \xrightarrow{\infty} 0$, we can compactify $\mathbb{R}^2$ onto the unit sphere S^2 and perform the integration with $\mathcal{M} = S^2$. This is equivalent to solving the integral with $\mathcal{M} = \mathbb{R}^2$ and dropping the surface term at infinity by using the anomalous divergence of J^5_μ (cf. section 4.7.2 in [4]), thus

$$\mathrm{ind}D_+ = \frac{q_e}{2\pi}\int_{S^2}\frac{1}{2}F_{\mu\nu}\mathrm{d}x^\mu\mathrm{d}x^\nu = \frac{q_e}{4\pi}\int_{S^2}{}^*F\varepsilon_{\mu\nu}\mathrm{d}x^\mu\mathrm{d}x^\nu = \frac{q_e}{4\pi}\int \mathrm{d}^2x\,\varepsilon^{\mu\nu}F_{\mu\nu}, \tag{1.87}$$

which is in consonance with Fujikawa's computation of the chiral anomaly. Thus, we can employ a topological result to compute the chiral anomaly associated with this U(1) gauge theory.

1.5 Anomaly and the fermion spectrum

1.5.1 Schwinger model on a circle

Let us consider a system with a Lagrangian given by (1.3) on a one-dimensional universe of length L compactified into a circle S^1. We can impose periodic boundary conditions on the A_μ field and antiperiodic boundary conditions to the fermions ψ

$$\begin{aligned} A_\mu(t, x = -L/2) &= A_\mu(t, x = L/2) \\ \psi(t, x = -L/2) &= -\psi(t, x = -L/2). \end{aligned} \tag{1.88}$$

Moreover, we can work in a gauge where $A_0 = 0$ and choose $A_1(t)$ as an *external field* which can be treated as an adiabatic perturbation to the system. As a consequence of the gauge freedom

$$A_\mu \to A_\mu + \partial_\mu\Lambda(x,t), \quad \psi \to e^{i\Lambda(t,x)}\psi$$

The gauge transformation $\Lambda(x,t)$ can be chosen to be

$$\Lambda(x,t) = \frac{2\pi}{L} nx; \quad n = \pm 1, \pm 2, \dots \tag{1.89}$$

which is in accordance with the boundary conditions imposed in (1.88) since $\partial_x \Lambda(x,t) = \text{const}$ and $\partial_t \Lambda(x,t) = 0$. Which means that neither the periodic nature of A_1 nor the anti-periodic nature of ψ are violated by the gauge function, since the phase factor at $-L/2$ and $L/2$ is a multiple of $2\pi n$. As a result of this, the physically meaningful values of A_1 are restricted to the interval $[0, 2\pi/L]$, since values outside this interval are gauge equivalent to a point inside the interval. This implies that the gauge field A_1 lives in a circle of length $2\pi/L$ where it takes physical values.

The Lagrangian of the theory is invariant under a $U(1)$ symmetry

$$\begin{aligned} \psi &\to e^{i\Lambda(x)}\psi \\ \bar{\psi} &\to \bar{\psi} e^{-i\Lambda(x)} \end{aligned} \tag{1.90}$$

which gives rise to the conservation of electric charge and vector current

$$\partial_\mu J^\mu = 0, \quad \dot{Q}(t) = 0 \tag{1.91}$$

with

$$Q(t) = \int \mathrm{d}x\, J_0(t,x). \tag{1.92}$$

Additionally it has an axial symmetry $U_A(1)$

$$\begin{aligned} \psi &\to e^{i\beta(x)\gamma_5}\psi \\ \bar{\psi} &\to \bar{\psi} e^{i\beta(x)\gamma_5} \end{aligned} \tag{1.93}$$

which yields the conservation of the axial current and the axial charge

$$\partial_\mu J^\mu_5 = 0, \quad \dot{Q}_5(t) = 0 \tag{1.94}$$

with

$$Q(t) = \int \mathrm{d}x\, J^5_0(t,x). \tag{1.95}$$

Classically both $Q(t)$ and $Q_5(t)$ are conserved.

Recalling the decomposition of the spinor in positive and negative chiralities (1.74) then the axial charge of the positive chirality spinor is $Q_5^+ = +1$ and the one for the negative chirality spinor is $Q_5^+ = -1$. Therefore, the conservation of both Q and Q_5 implies the *classical* conservation of the number of the positive and negative chirality particles separately. However, quantum mechanically both (1.92) and (1.95) cannot be conserved simultaneously as a consequence of the *chiral anomaly* and only $Q(t)$ is conserved after quantization.

In 1+1 dimensional QED, choosing a representation of the gamma matrices as (1.6), the Dirac equation is written as

$$[i(\gamma^0\partial_t + \gamma^1\partial_x) + q_e(\gamma^0 A_0 + \gamma^1 A_1)]\psi = 0$$

which reduces to (recalling we have set $A_0 = 0$)

$$\partial_t\psi = -\sigma_3(i\partial_x - q_e A_1)\psi. \tag{1.96}$$

Due to the form of (1.96) and the boundary conditions (1.88) we can use a Fourier expansion of the spinors

$$\psi(t,x) = \frac{1}{\sqrt{L}}\sum_k u(k)e^{-iE_k t}\exp\left[i\left(k+\frac{1}{2}\right)\frac{2\pi}{L}x\right], \quad k\in\mathbb{Z} \tag{1.97}$$

which satisfies the following "stationary Schrödinger" equation

$$E_k \psi_k(x) = -\sigma_3 (i\partial_x - q_e A_1)\psi_k(x). \tag{1.98}$$

We can see that the energies for the k-th level of the positive and chirality spinors are respectively

$$E_k^- = \frac{2\pi}{L}\left(k + \frac{1}{2}\right) + q_e A_1 \tag{1.99}$$

$$E_k^+ = -\frac{2\pi}{L}\left(k + \frac{1}{2}\right) - q_e A_1. \tag{1.100}$$

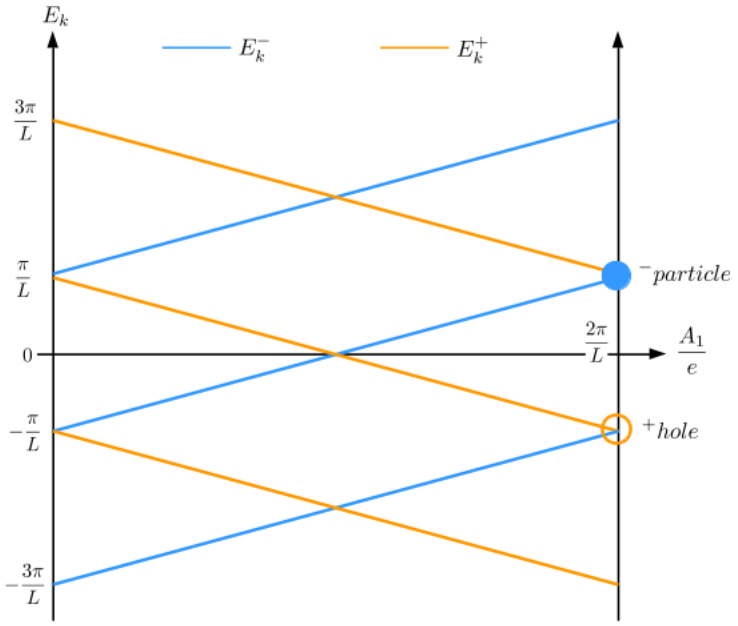

Figure 1.5.1: Fermion spectrum as function of A_1.

The spectrum is plotted in figure 1.5.1. We can see that the spectrum has a linear dependence on A_1. At $A_1 = 0$ the energy levels of the positive and negative chirality fermions are degenerate. However, as A_1 increases the energy levels split.

At $A_1 = 2\pi/L$ the degeneracy occurs again as expected since this point is gauge equivalent to $A_1 = 0$. Moreover, the restructuring of the spectrum when A_1 changes from 0 to $2\pi/L$ is non-trivial since the positive chirality levels are shifted downwards while the negative chirality levels are shifted upwards. This restructuring of the spectrum is the essence of the chiral anomaly.

1.5.2 Infrared and ultraviolet behavior

Let us now construct the ground state of the theory following Dirac's prescription of filling the Dirac sea while leaving all the positive energy levels empty. This can easily be done by looking at figure 1.5.1, viz

$$\left|\psi_{\text{vac}}\right\rangle = \left[\prod_{k=-1,-2,\ldots} \left|1_k\right\rangle_-\right]\left[\prod_{k=0,1,2,\ldots} \left|1_k\right\rangle_+\right] \tag{1.101}$$

where the 1 denotes either a positive or negative chirality level filled having momentum k as given, by (1.97). At $A_1 = 0$, by construction, we have a vacuum state of the fermions. Nevertheless, by increasing A_1 to $2\pi/L$ we produce, by the restructuring of the spectrum, a $^-$particle and a $^+$hole (represented by circles in figure 1.5.1). This energy level restructuring implies a net change in the conserved charges. The appearance of both a particle and a hole does not change the electric charge Q since the particle and the hole carry opposite electric charges. Nonetheless, the axial charges of the particle and the hole are identical ($Q_5 = 1$) and thus the restructuring of the spectrum induces a net change in Q_5 given by

$$\Delta Q_5 = 2. \tag{1.102}$$

This can be rewritten in terms of A_1 as

$$\Delta Q_5 = \frac{q_e L}{\pi}\Delta A_1, \tag{1.103}$$

we can divide it by Δt getting the following time evolution equation

$$\dot{Q}_5 = \frac{q_e L}{\pi}\dot{A}_1 \tag{1.104}$$

which written as the conserved quantity is

$$\frac{\partial}{\partial t}\int dx \left(J^5_0(x,t) - \frac{q_e}{\pi}A_1\right) = 0. \tag{1.105}$$

The current is given by

$$\bar{J}^5_\mu = J^5_\mu - \frac{q_e}{\pi}\varepsilon^{\mu\nu}A_\nu; \quad \partial^\mu \bar{J}^5_\mu = 0 \tag{1.106}$$

we have recovered the usual chiral anomaly result derived in section 1.3

$$\partial^\mu J^5_\mu = \frac{q_e}{2\pi}\varepsilon_{\mu\nu}\partial^\mu A^\nu. \tag{1.107}$$

Therefore, in this context, the anomaly presents as a result of the crossing of the energy levels at the energy $E = 0$ as a consequence of a variation of the value of the gauge filed A_1. This analysis is known as an *infrared* argument since it pertains low energies.

However, we can also study the anomalous behavior by introducing an *ultraviolet cutoff* to regularize the theory at high energy scales. The vacuum wavefunction being a superposition of infinitely many filled states of the Dirac sea is a divergent quantity. To obtain a sensible result, we have to introduce a gauge invariant regulator. A first naive idea for regularization is to impose a limit on the number of modes such that $k \in [-k_{\max}, k_{\max}]$, however, this type of regularization breaks gauge invariance and electric charge conservation. A regularization procedure that preserves gauge invariance is the gauge invariant point-splitting method due to Schwinger [11]. In this scheme, we can introduce the regularized currents that avoid the divergences of the form

$$J^{\mu}_{\text{reg}} = \lim_{\varepsilon \to 0} \bar{\psi}(t, x+\varepsilon)\gamma^{\mu}\psi(t,x) \exp\left(iq_e \int_x^{x+\varepsilon} \mathrm{d}x\, A_1\right),$$
$$J^{\mu}_{5\,\text{reg}} = \lim_{\varepsilon \to 0} \bar{\psi}(t, x+\varepsilon)\gamma^{\mu}\gamma_5\psi(t,x) \exp\left(iq_e \int_x^{x+\varepsilon} \mathrm{d}x\, A_1\right) \tag{1.108}$$

The new regularized charges are therefore defined to be

$$Q^{\text{reg}}(t) = \int \mathrm{d}x\, J^{\text{reg}}_0(t,x)$$
$$Q^{\text{reg}}_5(t) = \int \mathrm{d}x\, J^{\text{reg}}_{0\,5}(t,x), \tag{1.109}$$

and for the charges of the positive and negative chirality spinors

$$Q_- = \frac{Q - Q_5}{2}$$
$$Q_+ = \frac{Q + Q_5}{2}. \tag{1.110}$$

Using the regularized current expression (1.108) and the Fourier expansion of the spinors, we can calculate the positive and negative chirality charges explicitly yielding the following sums over k

$$Q_- = \sum_{k=-1}^{-\infty} \exp\left(-i\varepsilon\left[\left(k+\frac{1}{2}\right)\frac{2\pi}{L} - q_e A_1\right]\right)$$
$$Q_+ = \sum_{k=0}^{\infty} \exp\left(-i\varepsilon\left[\left(k+\frac{1}{2}\right)\frac{2\pi}{L} - q_e A_1\right]\right). \tag{1.111}$$

The summations for Q_+ and Q_- run over a different sets of k's as one can see from figure 1.5.1 and from equation (1.101). The negative chirality Dirac sea is field with modes $k = -1, -2, \ldots$, while the positive chirality Dirac sea is filled

with modes $k = 0, 1, 2, \ldots$. Doing the summation and the expanding in ε we can study the divergent part of both Q_- and Q_+, viz

$$\begin{aligned} Q_- &= -\frac{L}{2\pi}\frac{1}{i\varepsilon} + \frac{q_e L}{2\pi}A_1 + \mathcal{O}(\varepsilon) \\ Q_+ &= \frac{L}{2\pi}\frac{1}{i\varepsilon} - \frac{q_e L}{2\pi}A_1 + \mathcal{O}(\varepsilon). \end{aligned} \tag{1.112}$$

The physical charges of the theory are Q and Q_5. These are defined in terms of Q_- and Q_+ as

$$Q = Q_- + Q_+; \quad Q_5 = Q_+ - Q_- \tag{1.113}$$

hence, by using result (1.112) we find that in fact, the electric charge Q is conserved

$$\Delta Q = 0. \tag{1.114}$$

Nevertheless, the chiral charge Q_5 has a net change of

$$\Delta Q_5 = 2\frac{L}{2\pi}A_1. \tag{1.115}$$

Whenever the value of A_1 varies from 0 up to $2\pi/L$, this is consistent with the result already presented in subsection 1.5.2.

This analysis suggests to us a different interpretation of the chiral anomaly in the Schwinger model. Previously, the anomaly presented itself as a non-conservation of the chiral charge due to the fermion spectrum restructuring. The energy levels of fermions and anti-fermions cross the zero point energy of the vacuum creating a net excess of chiral charge. Nevertheless, by analyzing the ultraviolet behavior of the model we can note that the chiral charge non-conservation is a consequence of the energy levels crossing the ultraviolet cut-off ε we imposed to regularize the physically relevant quantities. Note that both the crossing of the levels at the vacuum energy and the departure beyond the ultraviolet cut-off are simultaneous processes.

Hence, both the infrared and ultraviolet analyses are adequate to explain the physics of the anomaly as a dynamic restructuring of the energy level of the Dirac spectrum.

1.6 Comments and conclusion

Throughout this chapter, we have studied various important physical aspects of quantum electrodynamics in $(1+1)$-dimensions, i.e. the Schwinger model. In the first section 1.2 we derived the equations of motion of the theory which are the *Dirac equation* and *Maxwell's equations*, also we computed the *Hamiltonian* of the theory, which will be very important later on within this thesis. Using the equations of motion, the simplicity of electrodynamics in one spatial dimension, and the anomalous divergence of the axial Noether current we showed that the theory has a massive "photon" whose mass is given in terms of the electromagnetic coupling constant, viz

$$m_\gamma = \frac{q_e}{\sqrt{\pi}}.$$

Let us stop for a moment and comment on the relevance of this. We started with QED in $(1+1)$-dimensions, where the photon is massless as it is expected from Maxwell's equations. Nevertheless, we found that as a consequence of the chiral anomaly of the model, resulting from the $U_A(1)$ symmetry associated to the chirality of the fermions the photon has acquired a non-zero mass. Therefore, the incompatibility of chiral symmetry with the quantization of the theory, i.e. the chiral anomaly, has generated a Higgs-like mechanism of "dynamic" mass generation (dynamic since it is realized at the level of the equations of motion) for the photon, where its mass follows immediately from breaking of the classical axial symmetry. Furthermore, this can also be understood as a result of the Coulomb's potential being linear with the distance $\boldsymbol{r}$ between the charges in $D = 2$, which makes the theory a *confining* one, much like QCD_4. Thus, we can make the "heuristic" argument (since a formal argument would be outside the scope of this thesis) that the theory develops a mass gap. In fact, the theory is equivalent of a free massive

scalar particle of mass m_γ where this massive particle is interpreted as a bound state of a fermion anti-fermion pair [2].

Additionally, in subsection 1.2.1 we explored how in one spatial dimension the presence of a background electric field $\mathcal{E}$ induces vacuum pair production which due to the energetics of this phenomenon in one dimension creates a discontinuity in the vacuum energy density (cf. figure 1.2.2) as a function of the ratio of background electric field and the electron charge $\mathcal{E}_0 \doteq \mathcal{E}/q_e$. This discontinuity in the energy density is a characteristic sign of a first order phase transition and this is a very interesting phenomenon we will later explore.

In the second section 1.3, we derived how the chiral anomaly of the Schwinger model arises as a consequence of a non-trivial Jacobian factor appearing in the fermionic path integral measure related to an infinitesimal $U_A(1)$ symmetry transformation of the classical action

$$\mathcal{D}\psi\mathcal{D}\bar{\psi} \to \mathcal{D}\psi'\mathcal{D}\bar{\psi}' = J[\beta]\mathcal{D}\psi\mathcal{D}\bar{\psi}.$$

This Jacobian was calculated using a covariant ultraviolet regulator and was found to be proportional to the pseudoscalar operator $\varepsilon_{\mu\nu}F^{\mu\nu}$. This result together with the Schwinger-Dyson equation for the chiral symmetry transformation yields the anomalous divergence of the axial current

$$\partial_\mu \left\langle J^\mu_5 \, \mathcal{O}(x_1 \dots x_n) \right\rangle = \frac{q_e}{2\pi} \left\langle \varepsilon^{\mu\nu} F_{\mu\nu} \, \mathcal{O}(x_1 \dots x_n) \right\rangle$$

Additionally, in regards to the anomaly, we showed how it stems from a purely topological consideration concerning the index of the Dirac operator which can be computed directly using the Atiyah-Singer index theorem for the Dirac operator coupled to a $U(1)$ gauge field namely:

$$\frac{q_e}{4\pi} \int \mathrm{d}^2x \, \varepsilon_{\mu\nu} F^{\mu\nu} = \mathrm{ind} D_+.$$

Finally, in section 1.5 we discussed briefly how the chiral anomaly derived previously has an effect on the fermion spectrum. To this end, we focus on the Schwinger model on a circle. In this context, due to translational invariance, we can use the Fourier mode decomposition of the fermion and gauge fields. Using the Fourier form of the fields together with the Dirac equation, we showed that the energy levels for the two components of the spinors change linearly with the gauge field A_1. Moreover, due to the gauge symmetry of the electromagnetic field, its values are restricted to a circle of length $2\pi/L$ and as such by varying the values in this range, the spectrum of the Dirac operator suffers a non-trivial restructuring. Due to this restructuring some of the energy levels close to the Dirac sea energy cross the low energy Dirac sea level, effectively creating a particle-hole pair from the vacuum (cf. figure 1.5.1) and inducing a net change in the axial charge Q_5. Likewise, this restructuring of the energy levels as a consequence of a change in A_1 happens in the high energy regime, where we introduced a cutoff to regularize the physically relevant quantities. This restructuring of the spectrum implies in particular that a level will depart from the ultraviolet cutoff boundary while a new level will appear within this boundary (cf. figure 1.5.1) yielding a non-conservation of the axial charge. Indeed, both these low and high energy descriptions, are the essence of the chiral anomaly.

To conclude, throughout this chapter we have explored the continuum Schwinger model and some of its most relevant and most interesting physical aspects. We showed the model has a chiral anomaly due to a $U(1)$ symmetry breaking. Furthermore, we computed the exact value of the anomalous current and explored the various physical consequences the anomaly has on the spectrum of the theory and the associated conserved charges of the model.

2

Spin chains

2.1 Motivation and Introduction

Many-body systems are usually quite difficult or even impossible to solve analytically due to the insurmountable difficulties in the calculations associated with the staggering number of degrees of freedom a system has. Nonetheless, quantum spin chain models are a class of (often) integrable systems in 1 spatial dimension with very rich physics. The paradigmatic spin chain model is the Heisenberg model introduced simultaneously by Paul Dirac and Werner Heisenberg, hence its name, in 1928 [12]. It is a model of interacting quantum spin-1/2 particles in a one-dimensional lattice conceived as a model for ferromagnetism. This model has critical points where it exhibits quantum phase transitions, analogous to classical phase transitions but at temperature $T = 0$. This fact makes it a very interesting model to study. The spin-1/2 Heisenberg model in one dimension was first solved by Hans Bethe

in 1931 [13] by using a plain wave ansatz known as the Bethe ansatz.

Of particular interest in this thesis is a special case of the Heisenberg model, the one-dimensional XY-model. This model has a very interesting phase diagram with two quantum phase transitions from separate universality classes, the Ising universality class with central charge $c = 1/2$ and the Heisenberg universality class with central charge $c = 1$. A solution of the model without a transverse magnetic field was first presented in a seminal paper by Lieb, Mattis and Schultz [14] in 1961, and shortly after the solution with a transverse magnetic field was presented by Neimeijer and Ruijgrok [15]. After the Neimeijer and Ruijgrok in a titanic series of papers, Barouch and McCoy solved the statistical mechanics of the model completely [16, 17], cementing this model as the paradigmatic physical system for studying quantum phase transitions and quantum dynamics. In recent years, however, the XY-model is being studied in the context of entanglement dynamics and out of equilibrium dynamics within the quantum information science community [18, 19].

In this chapter, we present the solution of the XY-model and compute its spectrum analytically. We follow the usual procedure of first introducing Jordan-Wigner transformation, followed by a Fourier transform and finally a Bogoliubov rotation. We study the structure of the ground state and discuss the model's very rich phase diagram. Additionally, we make special emphasis on the case where the model reduces to the XX-model since it will be key in the next chapter. We discuss the XX-spectrum, its ground state and compute the ground state energy density in the thermodynamic limit.

The reader might be wondering why we will make a detour and devote a full chapter to the solution of the XY-model when the title of this thesis makes no mention to spin chains or the XY-model. However, this will be done as to freely borrow results from the solution of the XY-model throughout the following chapter. Why will we need this results in future chapters will become clear shortly, however,

at this stage we can say that the discrete form of the Dirac equation yields, under certain conditions, a Hamiltonian equivalent to the XX-model.

2.2 The XY-model in a transverse field

The XY-model is a one-dimensional quantum many-body model and a special case of the Heisenberg spin chain model. It is described by the Hamiltonian

$$H(\gamma, g) = J \sum_{n=1}^{N} \left[\frac{1+\gamma}{2} \sigma_n^x \sigma_{n+1}^x + \frac{1-\gamma}{2} \sigma_n^y \sigma_{n+1}^y \right] - \frac{g}{2} \sum_{n=1}^{N} \sigma_n^z \tag{2.1}$$

where $0 \leq \gamma \leq 1$ is known as the anisotropy parameter. We can choose $\gamma = 0$ yielding the isotropic XX-model or $\gamma = 1$ yielding the transverse field Ising model. The sign of the coupling J determines whether the chain is ferromagnetic ($J < 0$), i.e. the spins tend to align, or antiferromagnetic ($J > 0$) and the spins tend to be anti-aligned. The standard way to tackle a Hamiltonian like (2.1) is to map the spin-1/2 operators to a set of spinless fermionic operators using a Jordan-Wigner transformation

$$\begin{aligned} \sigma_n^x &= \left[\prod_{l<n} \sigma_l^z \right] (\varphi_n^\dagger + \varphi_n) \\ \sigma_n^y &= i \left[\prod_{l<n} \sigma_l^z \right] (\varphi_n^\dagger - \varphi_n) \\ \sigma_n^z &= (1 - 2\varphi_n^\dagger \varphi_n) \end{aligned} \tag{2.2}$$

such that the set $\{\varphi_n\}_{n=1,\ldots,N}$ obeys the usual CAR algebra

$$\{\varphi_i, \varphi_j^\dagger\} = \delta_{ij} \quad \{\varphi_i, \varphi_j\} = \{\varphi_i^\dagger, \varphi_j^\dagger\} = 0. \tag{2.3}$$

By virtue of the Jordan-Wigner transformation, the eigenstates of σ^z, $|\uparrow\rangle$ and $|\downarrow\rangle$

are mapped into $|0\rangle$ and $|1\rangle$, which represent the presence or absence of a fermion in each lattice site. Applying the transformation to Hamiltonian (2.1) yields

$$H(J,\gamma,g) = J\sum_{n=1}^{N}\left[\varphi_n^\dagger\varphi_{n+1} + \varphi_{n+1}^\dagger\varphi_n + \gamma\left(\varphi_n^\dagger\varphi_{n+1}^\dagger + \varphi_{n+1}\varphi_n\right)\right] + 2g\sum_{n=1}^{N}\varphi_n^\dagger\varphi_n - \frac{gN}{2}. \tag{2.4}$$

We can ignore the constant term $gN/2$ since it is a simple energy offset that is irrelevant to the physics of the system.

This Hamiltonian can be diagonalized using a combination of Fourier and Bogoliubov transformations. First, let us introduce the momentum representation of the fermionic operators, namely

$$\varphi_k = \frac{1}{\sqrt{N}}\sum_l \varphi_l e^{-ik_n l}; \quad k_n = \pi\left(\frac{2n+1}{Na}\right), \quad n = 0, \pm 1, \ldots, \pm N, \tag{2.5}$$

Where a is the lattice spacing. The momentum k_n lies in the set $[-\pi/a, \pi/a]$. Additionally, the condition that the Fourier transformed operators satisfy the CAR algebra plus the condition of being in the even parity sector (as we are interested in the ground state) fixes the values of the k_n's in (2.5). In the Fourier basis, the Hamiltonian can be neatly written as the almost diagonal form

$$H(J,\gamma,g) = \sum_{k>0}\left[(g - J\cos k_n)\varphi_k^\dagger\varphi_k - iJ\gamma\sin k_n\left(\varphi_k^\dagger\varphi_{-k}^\dagger + \varphi_k\varphi_{-k}\right)\right], \tag{2.6}$$

which is equivalent to the matrix form

$$H(J,\gamma,g) = \sum_k (\varphi_k^\dagger,\ \varphi_{-k})\begin{pmatrix} a(k_n) & -i\beta(k_n) \\ i\beta(k_n) & -a(k_n)\end{pmatrix}\begin{pmatrix}\varphi_k \\ \varphi_{-k}^\dagger\end{pmatrix}, \tag{2.7}$$

with $a(k_n) = g - J\cos(k_n)$ and $\beta(k_n) = J\gamma\sin(k_n)$. This form of the Hamiltonian

suggests that in order to diagonalize it we should make use of a Bogoliubov transformation that only mixes $\varphi_k^\dagger$ with $\varphi_{-k}^\dagger$. Hence, the correct transformation is

$$\eta_k = u_k(\gamma, g)\varphi_k - iv_k(\gamma, g)\varphi_{-k}^\dagger, \quad \eta_{-k} = u_k(\gamma, g)\varphi_{-k} + iv_k(\gamma, g)\varphi_k^\dagger \tag{2.8}$$

where the η_k represent the new Bogoliubov fermions. The old fermions are given in terms of the inverse transformation

$$\varphi_k = u_k(\gamma, g)\eta_k + iv_k(\gamma, g)\eta_{-k}^\dagger, \quad \varphi_{-k} = u_k(\gamma, g)\eta_{-k} - iv_k(\gamma, g)\eta_k^\dagger. \tag{2.9}$$

The transformation coefficients $u(\gamma, g), v(\gamma, g)$ being real and the unitarity of the transformation enforces the conditions that $u_k^2(\gamma, g) + v_k^2(\gamma, g) = 1$. This fact suggests to us the parametrization

$$u_k(\gamma, g) = \cos\left(\frac{\theta_k}{2}\right), \quad v_k(\gamma, g) = \sin\left(\frac{\theta_k}{2}\right). \tag{2.10}$$

Applying the transformation yields the following Hamiltonian

$$H(J, \gamma, g) = \sum_k (\varphi_k^\dagger,\ \varphi_{-k}) \begin{pmatrix} u_k & iv_{-k} \\ -iv_k & u_{-k} \end{pmatrix} \begin{pmatrix} a(k_n) & -i\beta(k_n) \\ i\beta(k_n) & -a(k_n) \end{pmatrix} \begin{pmatrix} u_k & iv_{-k} \\ -iv_k & u_{-k} \end{pmatrix}^{-1} \begin{pmatrix} \varphi_k \\ \varphi_{-k}^\dagger \end{pmatrix}. \tag{2.11}$$

The objective of applying the Bogoliubov rotation is to make the off-diagonal terms vanish, and as such enforcing the requirement that the coefficients of the off-diagonal terms vanish leads to the condition

$$\frac{u_k v_k}{u_k^2 + v_k^2} = \frac{J\gamma \sin(k_n)}{g - J\cos(k_n)}, \tag{2.12}$$

provided that both u_k and v_k are eigenstates of the Bogoliubov- de Gennes equations

$$\begin{pmatrix} a(k_n) & -i\beta(k_n) \\ i\beta(k_n) & -a(k_n) \end{pmatrix} \begin{pmatrix} u_k \\ v_k \end{pmatrix} = \varepsilon_k \begin{pmatrix} u_k \\ v_k \end{pmatrix}. \tag{2.13}$$

Equation (2.13) implies there are two eigenstates for each k with single particle energies given by

$$\varepsilon_k = \pm\sqrt{(g - J\cos(k_n))^2 + (J\gamma\sin(k_n))^2}. \tag{2.14}$$

Note that applying the Bogoliubov transformation together with the parametrization (2.10) diagonalizes the Hamiltonian provided that the Bogoliubov angles satisfy

$$\begin{aligned} \tan(\theta_k) &= \frac{J\gamma\sin(k_n)}{g - J\cos(k_n)} \\ \sin(\theta_k) &= \frac{J\gamma\sin(k_n)}{\sqrt{(g - \cos(k_n))^2 + (J\gamma\sin(k_n))^2}} \\ \cos(\theta_k) &= \frac{g - J\cos(k_n)}{\sqrt{(g - \cos(k_n))^2 + (J\gamma\sin(k_n))^2}}, \end{aligned} \tag{2.15}$$

or equivalently

$$e^{i\theta_k} = \frac{g - J\cos k_n + iJ\gamma\sin k_n}{\sqrt{(g - J\cos k_n)^2 + (J\gamma\sin k_n)}}. \tag{2.16}$$

Choosing the positive energy eigenstate from (2.14) the Hamiltonian is written as a diagonal form in terms of the Bogoliubov fermions, viz

$$H = \sum_k \varepsilon_k \left(\eta_k^\dagger \eta_k - \frac{1}{2}\right). \tag{2.17}$$

2.2.1 The ground state

The ground state (or Bogoliubov vacuum) of the Hamiltonian (2.17) will be labeled $|\mathrm{GS}\rangle$. Having brought the Hamiltonian to the diagonal form, the ground state will be given by the condition

$$\eta_k |\mathrm{GS}\rangle = 0 \quad \forall k. \tag{2.18}$$

However, let us consider the "vacuum" state $|0\rangle$ for the φ-fermions, which is defined by the condition

$$\varphi_k |0\rangle = 0 \quad \forall k. \tag{2.19}$$

Let us note that we can define

$$B_k \doteq u_k(g) + i v_k(g) \varphi_k^\dagger \varphi_{-k}^\dagger \tag{2.20}$$

with $u_k(g)$ and $v_k(g)$ the Bogoliubov coefficients (2.10). Moreover, this definition implies that

$$\varphi_k B_k |0\rangle_\varphi = 0.$$

Therefore, we can rewrite the ground state as a product of all the different B_k's, viz

$$|\mathrm{GS}\rangle = \prod_{k>0} \left(u_k(g) + i v_k(g) \varphi_k^\dagger \varphi_{-k}^\dagger \right) |0\rangle_\varphi . \tag{2.21}$$

Hence, equation (2.21) tells us that $|\mathrm{GS}\rangle$ contains an even number of φ-fermions that are always created as particle pairs with momenta $(k, -k)$.

2.2.2 The Phase Diagram

The zero temperature phase diagram of the XY-model in parameter space (γ, g) is depicted in figure 2.2.1. It is interesting to note that we can identify several critical regions of the parameter space where the spectrum (2.14) is zero. In particular, this implies that the gap vanishes and low energy quasi-particles dominate the behavior

of the system.

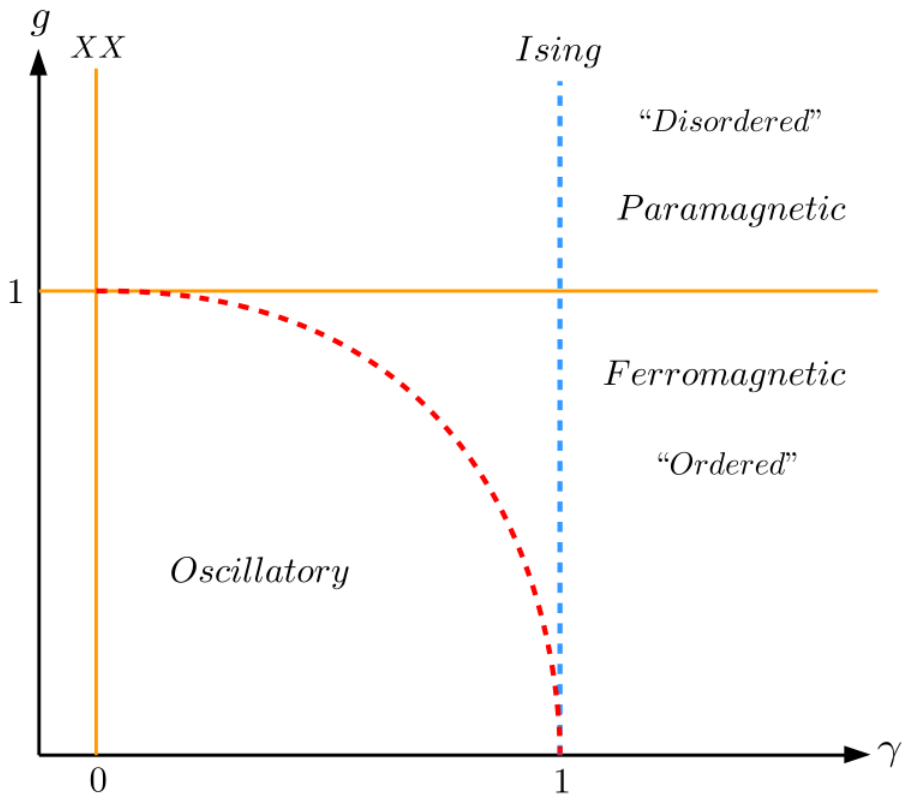

Figure 2.2.1: Phase diagram of the XY-model for γ and g positive.

Figure 2.2.1 shows the critical lines, $\gamma = 0$ which corresponds to the isotropic XY-model more commonly known as the XX-model. The line $g = 1$ is a critical line of the XY-model due to the transverse magnetic field. At the intersection of this line with the line $\gamma = 1$ lies the critical point of the transverse field Ising model. Below the $g = 1$ line the ground state is a doubly degenerate having a $\mathbb{Z}_2$ symmetry. In the ferromagnetically ordered phase $g < 1$, this $\mathbb{Z}_2$ symmetry is broken yielding a two-fold degeneracy in the ground state given by two states of opposite longitudinal magnetization

$$|\psi_1\rangle = |\rightarrow \ldots \rightarrow\rangle = \prod_{l=1}^{N} \frac{1}{\sqrt{2}}[|\uparrow\rangle_l + |\downarrow\rangle_l],$$
$$|\psi_2\rangle = |\leftarrow \ldots \leftarrow\rangle = \prod_{l=1}^{N} \frac{1}{\sqrt{2}}[|\uparrow\rangle_l - |\downarrow\rangle_l]. \tag{2.22}$$

The region $g > 1$ has a single ground state where all the spins are aligned with the transverse field. Finally, the line defined by $\gamma^2 + g^2 = 1$ corresponds to a region where the ground state wavefunction can be written aa product over single spin states.

2.3 The XX-model

The XX model corresponds to the special case of the XY-model when $\gamma = 0$. In which case the Hamiltonian is already diagonal after the Fourier transform as seen from equation (2.6). Thus, the Hamiltonian for the XX model after the Fourier transform reads

$$H_{XX}(J, g) = \sum_{k>0} (g - J\cos k_n)\varphi_k^\dagger \varphi_k, \tag{2.23}$$

from which we can immediately read the single particle energy dispersion relation to be

$$\varepsilon_k = g - J\cos(k_n). \tag{2.24}$$

The single particle energy spectrum is shown in figure 2.3.1. For $g > J$ the spectrum is positive and the ground state contains no fermions. However, for $J > g$ the spectrum has negative energy states corresponding to fermions with $k < |\cos^{-1}(g/J)|$.

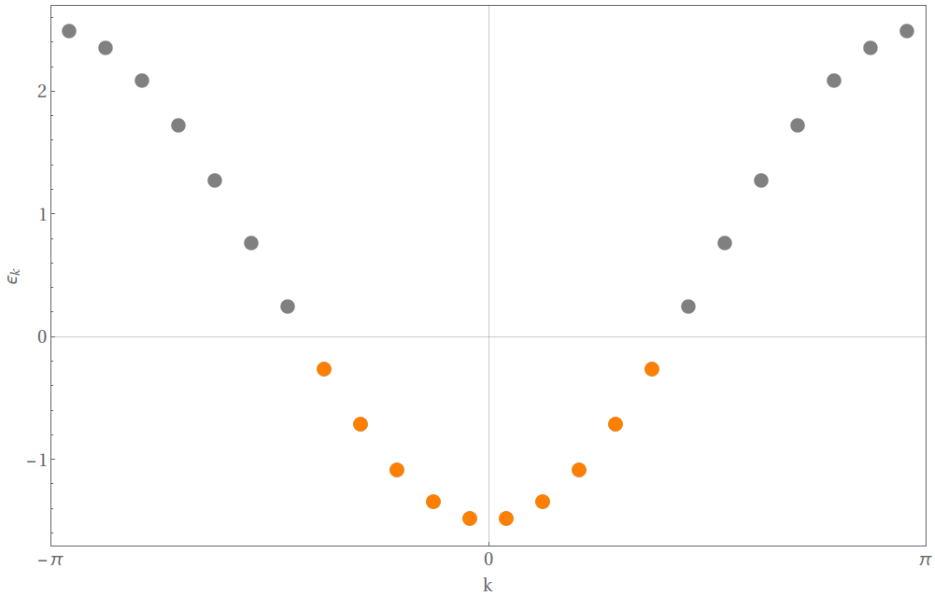

Figure 2.3.1: $N = 24$ XX-model spectrum for $g = 1/2$ and $J = 1$. The orange dots are filled Dirac sea states of the ground state.

The standard procedure is to fill the negative energy states, i.e. the Dirac sea in order to define the ground state of the system

$$|\mathrm{GS}\rangle = \prod_{k<\left|\cos^{-1}\left(\frac{g}{J}\right)\right|} \varphi_k^\dagger |\mathrm{o}\rangle \,, \tag{2.25}$$

with $|\mathrm{o}\rangle$ being the vacuum state of the fermions. This ground state corresponds to a spin chain with a half-filled band. Excited states above the ground state in this spin system correspond to adding a fermion with $k > |\cos^{-1}(g/J)|$ or annihilating one with $k < |\cos^{-1}(g/J)|$ to form a hole.

In the limit $N \to \infty$ we can compute the ground state energy per spin by replacing summations with integrals

$$\frac{E_\mathrm{o}}{N} = -\frac{1}{2}\sum_k |\varepsilon_k| \to \frac{E_\mathrm{o}}{N} = -\frac{1}{2}\int_{-\pi}^{\pi} \frac{\mathrm{d}k}{2\pi}\,\mathrm{d}k\,|\varepsilon_k|, \tag{2.26}$$

which after integration yields

$$\frac{E_0}{N} = -\frac{2\sqrt{1-g^2} + \pi g - 2g\cos^{-1}(g)}{2\pi}.$$

For the special case of zero transverse field, $g = 0$ the ground state energy reduces to

$$\frac{E_0}{N} = -\frac{1}{\pi} \tag{2.27}$$

This value will be very useful to us in the next chapter as we will use it as a benchmark in the various computer simulations of the model.

2.4 Comments and conclusion

Throughout this chapter, we have delved into the complete analytical solution of the XY-model in a transverse field. The solution presented in this chapter is the standard solution where the spin Hamiltonian is first mapped to a spinless fermion Hamiltonian by means of the Jordan-Wigner transformation. After the Jordan-Wigner transformation and taking advantage of the translation symmetry of the system, we diagonalized the Hamiltonian by introducing a Fourier transform followed by Bogoliubov rotation. This combination of unitary transformations fully diagonalized the fermion Hamiltonian. In this diagonal form, we find the single particle spectrum of the model to be

$$\varepsilon_k = \sqrt{(g - J\cos(k_n))^2 + (J\gamma\sin(k_n))^2}.$$

Additionally, by inspecting the ground state written in terms of the Fourier transformed fermions, we found that it is a state always composed by pairs of quasiparticle with opposite momenta

$$|\mathrm{GS}\rangle = \prod_{k>0}\left[\cos\left(\frac{\theta_k}{2}\right)|0\rangle_\varphi + i\sin\left(\frac{\theta_k}{2}\right)|k,-k\rangle\right].$$

Furthermore, in section 2.2.2 we briefly analyzed the phase diagram of the XY-

model (cf figure 2.2.1). We identified two critical lines, $\gamma = 0$ and $\gamma = 1$, that correspond to different universality classes, Ising universality, and Heisenberg universality class respectively. Also, we briefly commented on the structure of the ground state in each phase.

Finally, during section 2.3 we analyzed the XX-model, a special case of the XY-model with $\gamma = 0$. We computed its spectrum (cf. figure 2.3.1) and commented briefly on the structure of its ground state. The ground state had all of the negative energy states are filled following Dirac prescription of filling the Dirac sea. Furthermore, we calculated the ground state energy per spin, which in the special case of no transverse magnetic field reduces to

$$\frac{E_0}{N} = -\frac{1}{\pi},$$

this result will prove useful in the following chapters where the ground state energy of the free Schwinger model will be computed numerically.

3

The Schwinger model in a lattice

3.1 Motivation and Introduction

Lattice models in physics are versions of continuum field theories which are discretized to a lattice with the objective of making them useful for computer simulations. The motivation of this discretization procedure is that most quantum field theories are not exactly solvable and thus computer simulations can yield a great physical insight into the continuum theory. The aim is to take increasing system sizes while reducing the lattice spacing hoping that for a sufficiently fine discretization the continuum behavior of the model can be recovered. Moreover, numerical simulations can give access to non-trivial field configurations and vacuum states which are non-perturbative. The lattice version of gauge theory is particularly useful since gauge invariance is kept manifest at the Hamiltonian level [20]. The Schwinger model being a simple gauge theory is appealing to the methods of lattice gauge theory, and

thus the exploration of its lattice version will be very useful to study the dynamics of the system.

In this chapter, we will study the discrete version the Schwinger using Kogut-Susskind fermions [20, 21]. Using the Hamiltonian form of the theory (cf. equation (1.24)) we will construct lattice Hamiltonian. Furthermore, we will show the equivalence of this Hamiltonian to a spin chain model, and how in the case of the free Schwinger model the Hamiltonian coincides with the XX-model.

Moreover, we will discuss how gauge invariance fixes the form of the Hamiltonian describing the dynamics of the gauge field which turns out to be a quantum rotor. We show how the inclusion of the background field $\mathcal{E}_0$ follows straightforwardly from the continuum Hamiltonian and that the lattice model inherits the same critical behavior induced by the dynamics of particle anti-particle pair production present in the continuum model.

Finally, we show how Gauss's law fixes the subspace of physical states of the theory. This restriction imposed by gauge invariance permits the elimination of the gauge field from the Hamiltonian altogether. However, this introduces an effective mass term and a Coulomb interaction term to the lattice Hamiltonian. This formulation absent pf the gauge field variables will prove extremely useful in the next chapter were the computer simulations of the lattice system will be discussed.

3.2 Lattice formulation

The Schwinger model can be discretized on an N point lattice with lattice spacing a. We can work on either open, periodic or antiperiodic boundary conditions as seen in figures 3.2.1

Using the gamma matrices representation (1.7) the massless Dirac equation can

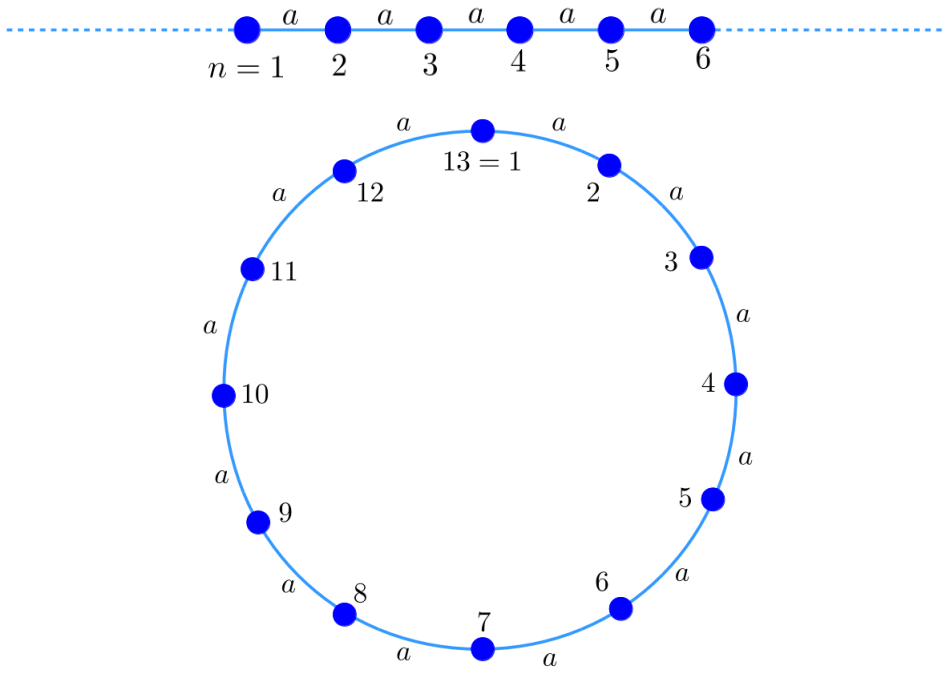

Figure 3.2.1: Lattice with open and periodic boundary condition.

be rewritten as

$$\partial_t \psi = \begin{pmatrix} 0 & 1 \\ 1 & 0 \end{pmatrix} \partial_x \psi. \tag{3.1}$$

We can replace the spatial derivative in (3.1) by a discrete difference

$$\partial_t \psi = \begin{pmatrix} 0 & 1 \\ 1 & 0 \end{pmatrix} \frac{1}{2a} [\psi(n+1) - \psi(n-1)], \tag{3.2}$$

and then we can reduce the number of degrees of freedom in each site by introducing one-component fermions φ on each lattice site. We demand that φ obeys equation (3.2). By using the Heisenberg equations of motion we find that φ must have the

following Hamiltonian

$$H = \frac{-i}{2a}\sum_n \left[\varphi_n^\dagger \varphi_{n+1} - \varphi_{n+1}^\dagger \varphi_n\right]. \tag{3.3}$$

Moreover, we can introduce Kogut-Susskind fermions [22] on a staggered lattice by defining even and odd sub-lattices which have independent fermion fields related to φ by

$$\begin{aligned} \psi_- &= \frac{1}{\sqrt{a}}\varphi_n, \quad n \text{ even} \\ \psi_+ &= \frac{1}{\sqrt{a}}\varphi_n, \quad n \text{ odd}, \end{aligned} \tag{3.4}$$

obeying

$$\partial_t \psi_\pm = \frac{1}{2a}\left[\psi_\pm(n+1) - \psi_\pm(n-1)\right]. \tag{3.5}$$

Since the lattice is a staggered one, translation symmetry is represented by a shift of even lattice sites namely:

$$\psi_\pm(n) \to \psi_\pm(n+m), \qquad m \bmod 2 = 0. \tag{3.6}$$

Within this formulation, fermion bilinears can be expressed in the lattice yielding

$$\begin{aligned} \psi^\dagger\psi &= \psi_-^\dagger(n)\psi_-(n) + \psi_+^\dagger(n)\psi_+(n) = \varphi_n^\dagger\varphi_n \\ \bar\psi\psi &= \psi_-^\dagger(n)\psi_-(n) - \psi_+^\dagger(n)\psi_+(n) = (-1)^n\varphi_n^\dagger\varphi_n. \end{aligned} \tag{3.7}$$

Equation (3.7), in particular, implies that a mass term in the Dirac equation $m\bar\psi\psi$ has the following lattice form

$$m\sum_n (-1)^n \varphi_n^\dagger \varphi_n. \tag{3.8}$$

3.2.1 Spin Hamiltonians

There exists a close connection between one-dimensional fermion chains and spin chains given by the Jordan-Wigner transformation. Let us think of a $1/2$-spin chain with Pauli spin operators $\sigma_n^{\pm}$ and σ_n^z, the Jordan-Wigner transformation

$$\begin{aligned} \varphi_n &= \left[\prod_{l<n} i\sigma_l^z\right]\sigma_n^+ \\ \varphi_n^\dagger &= \left[\prod_{l<n} -i\sigma_l^z\right]\sigma_n^- \end{aligned} \tag{3.9}$$

relates the fermion operators with the spin operators. Hence, the fermion Hamiltonian is equivalent to the following spin Hamiltonian

$$H = J\sum_n \left[\sigma_n^+\sigma_{n+1}^- + \sigma_{n+1}^+\sigma_n^-\right] = \frac{J}{2}\sum_n \left[\sigma_n^x\sigma_{n+1}^x + \sigma_n^y\sigma_{n+1}^y\right], \tag{3.10}$$

with $J = 1/2a$. Hamiltonian (3.10) is a special case of the XX-model Hamiltonian (with $\gamma = 0$ and $g = 0$) and whose solution we worked out in detail in chapter 2 (cf. section 2.2). Hamiltonian (3.10) is the lattice equivalent of the *free massless* Schwinger model.

In terms of spin matrices, Dirac bilinears are expressed as

$$\begin{aligned} \psi^\dagger\psi &= \frac{1}{2}\sigma_n^z, \\ \bar{\psi}\psi &= \frac{(-1)^n}{2}(1+\sigma_n^z), \\ \psi^\dagger\gamma_5\psi &= -i\left(\sigma_n^+\sigma_{n+1}^- - \sigma_{n+1}^+\sigma_n^-\right), \\ i\bar{\psi}\gamma_5\psi &= \left(\sigma_{n+1}^+\sigma_n^- + \sigma_n^+\sigma_{n+1}^-\right), \end{aligned} \tag{3.11}$$

which implies that both charge densities are written as

$$J^0 = \frac{1}{2}\left[\psi^\dagger, \psi\right] = \frac{1}{2}\sigma^z,$$
$$J^0_5 = \psi^\dagger \gamma_5 \psi = -i\left[\sigma^+_n \sigma^-_{n+1} + \sigma^+_{n+1}\sigma^-_n\right]. \tag{3.12}$$

A straightforward modification of (3.10) in virtue of (3.11) allows us to introduce the mass term, which in spin language is a staggered transverse field

$$H = J\sum_n \left[\sigma^+_n \sigma^-_{n+1} + \sigma^+_{n+1}\sigma^-_n\right] + \frac{m}{2}\sum_n (-1)^n \sigma^z_n. \tag{3.13}$$

This is the XY Hamiltonian with $\gamma = 0$ and a staggered transverse field with $g = m/2$. Hamiltonian (3.13) is the lattice equivalent of the *massive free* Schwinger model. Thus far, we have just introduced the fermion part of (1.24). This begs the question: how can we introduce the electromagnetic field in a gauge invariant manner?

To do so we use as inspiration the gauge invariant point-splitting method (1.108). In gauge invariant point splitting in order to preserve the gauge invariance, one must multiply by a phase factor that exactly cancels the transformation term picked up by the spinors. This phase factor is of the form

$$\exp\left[iq_e \int_x^{x+\varepsilon} \mathrm{d}x\, A_1\right].$$

Hence, following this prescription as a guide on how to proceed in the lattice we can on each link between lattice sites define the following operator

$$U(n; n+1) = e^{ia_n} \tag{3.14}$$

with $a_n = iaq_e A_1(n)$. This will be the parallel transporter operator associated to the $U(1)$ gauge field. Recall, we are working in the gauge $A_0 = 0$, which implies that the electric field $E = -\dot{A}_1$ is the canonical conjugate variable of A_1. In the

lattice formulation, this is equivalent to

$$[A_n, E_m] = iq_e\delta_{n,m}, \tag{3.15}$$

and from relation (3.15) we can define the following operator

$$L_n = \frac{E_n}{q_e}. \tag{3.16}$$

It follows from (3.15) that the physical range of a_n is (cf. section 1.5)

$$A_1 \in \left[0, \frac{2\pi}{q_e a}\right] \quad \Rightarrow \quad a_n \in [0, 2\pi]. \tag{3.17}$$

Also, it follows that L_n is an angular momentum operator which is quantized in integer values

$$L\,|n\rangle = l\,|l\rangle\,; \quad l = 0, \pm 1, \pm 2, \ldots. \tag{3.18}$$

Hence the electric field in the lattice version is represented by a *quantum rotor* in each link in between the fermions.

To render the Hamiltonian (3.13) gauge invariant, link operators U are introduced in the same spirit of gauge invariant point-splitting

$$J\sum_n \left[\sigma_n^+\sigma_{n+1}^- + \sigma_{n+1}^+\sigma_n^-\right] \to J\sum_n \left[\sigma_n^+ e^{ia_n}\sigma_{n+1}^- + \sigma_{n+1}^+ e^{-ia_n}\sigma_n^-\right], \tag{3.19}$$

namely the Hamiltonian reads

$$H = J\sum_n \left[\sigma_n^+ e^{ia_n}\sigma_{n+1}^- + \sigma_{n+1}^+ e^{-ia_n}\sigma_n^-\right] + \frac{m}{2}\sum_n (-1)^n\sigma_n^z. \tag{3.20}$$

Thus far, we have not introduced the dynamic Hamiltonian of the electric field. We introduce this term for the electromagnetic field to the lattice formulation following

Hamiltonian (1.24)

$$H = J\sum_n \left[\sigma_n^+ e^{ia_n}\sigma_{n+1}^- + \sigma_{n+1}^+ e^{-ia_n}\sigma_n^-\right] + \frac{m}{2}\sum_n (-1)^n\sigma_n^z + \xi\sum_n L_n^2, \quad (3.21)$$

with $\xi = q_e^2 a/2$. This is the lattice equivalent of the *fully interacting massive* Schwinger model.

3.2.2 Electric field operators and Hilbert space

Let us note that both a_n and A_1 only appear in the Hamiltonian trough $e^{\pm a_n}$. However, we need to determine how such operators act on the eigenstates of operator L_n. From the commutator (3.15) we have that

$$\begin{aligned} a_n L_n |l\rangle - L_n a_n |l\rangle &= i|l\rangle \\ l a_n |l\rangle - L_n a_n |l\rangle &= i|l\rangle . \end{aligned} \quad (3.22)$$

By acting upon (3.22) with a_n and using repeatedly (3.15) we arrive to a relation of the form

$$l(a_n)^k |l\rangle - L_n (a_n)^k |l\rangle = ik(a_n)^{k-1}|l\rangle .$$

If we multiply by $(\pm i)^k/k!$ and sum over all possible values of k we have that

$$l\sum_{k=1}^{\infty}\frac{(\pm i)^k}{k!}(a_n)^k|l\rangle - L_n\sum_{k=1}^{\infty}\frac{(\pm i)^k}{k!}(a_n)^k|l\rangle = \sum_{k=1}^{\infty}\frac{(\pm i)^k}{k!}ik(a_n)^{k-1}|l\rangle , \quad (3.23)$$

summing both the first and second sums form $k = 0$ and making the change k

to $k+1$ in the right-hand side sum we obtain that

$$l\sum_{k=0}^{\infty}\frac{(\pm i)^k}{k!}(a_n)^k\,|l\rangle - L_n\sum_{k=0}^{\infty}\frac{(\pm i)^k}{k!}(a_n)^k\,|l\rangle = \mp\sum_{k=0}^{\infty}\frac{(\pm i)^k}{k!}ik(a_n)^k\,|l\rangle\,, \quad (3.24)$$

finally, using the definition of the exponential of an operator this is equivalent to

$$(l\pm 1)e^{\pm ia_n}\,|l\rangle = L_n e^{\pm ia_n}\,|l\rangle\,. \quad (3.25)$$

Therefore, we note that

$$e^{\pm ia_n}\,|l\rangle = C\,|l+1\rangle\,. \quad (3.26)$$

If we further assume that states $|l\rangle$ form a complete orthonormal basis, then we can choose $C=1$. Hence, we have shown that the operators $e^{\pm ia_n}$ are the *raising (lowering) operators* of the eigenstates of L_n [22].

These results suggest that the relevant Hilbert space of the lattice model is a tensor product of the spin space and the L-space of the quantum rotor that represents the electromagnetic field, viz

$$\mathscr{H} = \bigotimes_{i=1}^{N}|s_i\rangle\otimes|l\rangle\,. \quad (3.27)$$

Here $s_i = \{\uparrow,\downarrow\}$ label the ± 1 eigenstates of σ^z and $l\in\mathbb{Z}$. As a consequence of the staggered nature of the lattice, an even site in spin state $|1\rangle$ has a fermion (an electron) while an odd site in spin state $|0\rangle$ corresponds to an anti-fermion (a positron).

3.2.3 The background field in the lattice

As it was discussed in section 1.2.1 very interesting physics arises when we consider the presence of a background electric field as a consequence of the dynamics of pair

production in one spatial dimension. The lattice version of the Schwinger model as described by the Hamiltonian (3.21) inherits this interesting physical behavior as well. The modification is simple, as it amounts to adding a single term in the Hamiltonian to account for the electrostatic energy of the background electric field, hence the kinetic term for the electromagnetic field is modified to

$$\xi \sum_n L_n^2 \to \xi \sum_n (L_n + \mathcal{E}_0)^2. \tag{3.28}$$

Thus, by virtue of this modification the physics of the lattice model in the presence of the background field corresponds exactly with the continuum model. If $\mathcal{E}_0 > 1/2$, pair production will begin and opposite charges separate the spatial edges lowering the electrostatic vacuum energy and bringing $\mathcal{E}_0$ below $1/2$. Therefore, at $\mathcal{E}_0 = 1/2$ a phase transition occurs between two degenerate ground states above the critical mass [23]

$$m_c = \frac{m}{q_e} = 0.3335(2). \tag{3.29}$$

In this context of spontaneous symmetry breakdown, we can study the dynamics of three order parameters that characterize the phase transition at $\mathcal{E}_0 = 1/2$. These are the axial fermion density

$$\Lambda = \langle i\bar{\psi}\gamma_5\psi \rangle = \frac{1}{Nq_e a} \left\langle \mathrm{GS} \left| \sum_n (-1)^n \left[\sigma_n^+ \sigma_{n+1}^- + \sigma_{n+1}^+ \sigma_n^- \right] \right| \mathrm{GS} \right\rangle, \tag{3.30}$$

and the density of chiral condensate

$$\Gamma = \langle \bar{\psi}\psi \rangle = \frac{1}{2Na} \left\langle \mathrm{GS} \left| \sum_n (-1)^n \sigma_n^z \right| \mathrm{GS} \right\rangle, \tag{3.31}$$

where $|\mathrm{GS}\rangle$ is the ground state associated to the Hamiltonian (3.21). These order parameters will be used in the following chapter concerning numerical computations of the lattice Schwinger model where computer simulations of small lattice systems

will be made to extract the value of these order parameters in various scenarios.

3.2.4 Gauss law

One of the paramount properties of the Schwinger model is the existence of *local gauge symmetries* associated with the gauge field A_1. Note that the state space of the model is a product of an infinite number of states of the electric field operator L_n on each link between lattice sites. Nevertheless, not all this states are physically relevant since we must enforce gauge invariance for the physical states. To do this, let us consider the generators of the gauge symmetries $\{G_i\}$ and how the Hamiltonian of the system transforms due to a gauge transformation

$$H' = \prod_i e^{i\beta_i G_i} H \prod_i e^{-i\beta_i G_i}, \tag{3.32}$$

where the β_i are some arbitrary set of parameters. This invariance is encoded in Gauss's law, which in the continuum model reads $\nabla \cdot E = \rho$. Nonetheless, in the Hamiltonian formulation of the lattice field theory Gauss's law can not be implemented as an operator identity but rather as an extra constraint [20]. In the lattice, the expression for the divergence of the electric field is given by the operator difference $L_n - L_{n-1}$, while charge density is $\psi^\dagger \psi$. Thus, for the lattice Schwinger model, the generators of the gauge symmetry group are

$$G_n = L_n - L_{n-1} - \psi_n^\dagger \psi_n + \frac{1 - (-1)^n}{2}. \tag{3.33}$$

The constant term is due to the staggered nature of the lattice. The Hamiltonian of the lattice model is gauge invariant by construction, i.e. $[H, G_I] = 0$. As it was mentioned before, the physical states of the theory should be eigenstates of the generators of gauge transformations

$$G_n \left|\psi_{\text{phys}}\right\rangle = q_n \left|\psi_{\text{phys}}\right\rangle, \tag{3.34}$$

where q_n's are external static charge distributions. Hence, the physical Hilbert space of the theory is a direct sum of sub-spaces labeled by different static charge

distributions.

Consequently, gauge invariance can be imposed by restricting the state space to a sector of fixed q_i by imposing (3.34). We can choose to work on the subspace of zero external charge, which means $G_i \left|\psi_{\text{phys}}\right\rangle = 0$. This is a state where there is an equal amount of particles and antiparticles in our one-dimensional universe, i.e. zero net charge. Now, we can rewrite equation (3.34) in terms of spin matrices by using the Jordan-Wigner transformation

$$L_n - L_{n-1} = \psi_n^\dagger \psi_n + \frac{1-(-1)^n}{2} = \frac{1}{2}[\sigma_n^z + (-1)^n]. \tag{3.35}$$

Moreover, by using equation (3.35) we can integrate out the gauge degrees of freedom from the gauge field and obtain a lattice Hamiltonian that acts only in the physical space of states. This means that we can express the electric field operators as

$$L_n = \mathcal{E}_0 + \frac{1}{2}\sum_l^N [\sigma_l^z + (-1)^l] \tag{3.36}$$

where $\mathcal{E}_0$ is the background electric field present in our one-dimensional universe. This is depicted in figure 3.2.2.

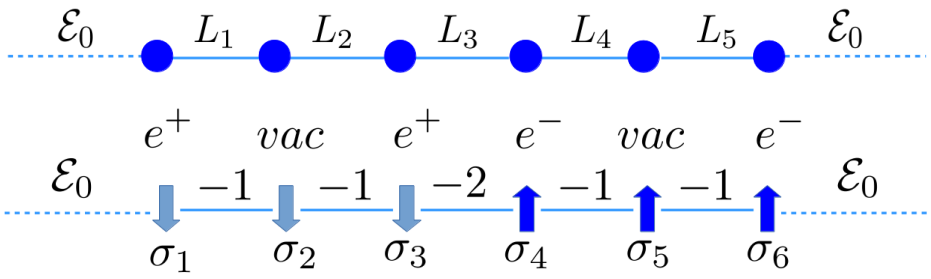

Figure 3.2.2: Lattice of $N = 6$ spins with the values of electric field L_n fixed by Gauss's law.

What is seen in figure 3.2.2 can be summarized as follows, on odd lattice sites

$$\uparrow = |0\rangle = \text{vacuum} \Rightarrow L_n = L_{n-1}; \quad \downarrow = |1\rangle = \psi_+ = e^+ \Rightarrow L_n = L_{n-1} - 1,$$

while on even lattice sites

$$\uparrow = |1\rangle = \psi_- = e^- \Rightarrow L_n = L_{n-1} + 1; \quad \downarrow = |0\rangle = \text{vacuum} \Rightarrow L_n = L_{n-1}.$$

Furthermore, by using relation (3.35) we can write the electric field Hamiltonian as

$$\xi \sum_n L_n^2 = \xi \sum_n \left(\mathcal{E}_0 + \frac{1}{2} \sum_{l=1}^{n} \left[\sigma_l^z + (-1)^l \right] \right)^2 . \tag{3.37}$$

Finally, in order to completely eliminate the operators $U(n; n+1)$, we can make the following gauge transformation

$$\sigma_n^- = \left[\prod_{l<n} e^{-i\alpha_n} \right] \sigma_n^-; \quad \sigma_n^+ = \left[\prod_{l<n} e^{i\alpha_n} \right] \sigma_n^+ . \tag{3.38}$$

Plugging transformed operators into the energy term to the electric field we obtain a Hamiltonian written completely in terms the spin content in the sites of the lattice, viz

$$H = J \sum_n \left[\sigma_n^+ \sigma_{n+1}^- + \text{h.c} \right] + \frac{m}{2} \sum_n (-1)^n \sigma_n^z + \xi \sum_n \left(\mathcal{E}_0 + \frac{1}{2} \sum_{l=1}^{n} \left[\sigma_l^z + (-1)^l \right] \right)^2 . \tag{3.39}$$

In this formulation where the gauge field has been integrated out using Gauss's law. The dynamics of the gauge field is replaced by non-local long-range spin-spin interactions that are an effective description of Coulomb's law in one spatial

dimension [24]

3.3 Effective mass and Coulomb interaction

Let us now explicitly compute the third term in the Hamiltonian[1] (3.39). Expanding the square we get

$$\xi \sum_{n=1}^{N-1} \left(\mathcal{E}_o^2 + \frac{1}{4} \left(\sum_{l=1}^{n} \left[\sigma_l^z + (-1)^l \right] \right)^2 + \mathcal{E}_o \sum_{l=1}^{n} \sigma_l^z \right), \tag{3.40}$$

the first term is a simple constant energy term we will ignore hereafter, as it is an energy offset that does not affect the physics of the system. The remaining two terms are

$$\xi \sum_{n=1}^{N-1} \frac{1}{4} \left(\sum_{l=1}^{n} \left[\sigma_l^z + (-1)^l \right] \right)^2 + \frac{m_{\mathcal{E}_o}}{2} \sum_{n=1}^{N-1} \sum_{l=1}^{n} \sigma_l^z, \tag{3.41}$$

with $m_{\mathcal{E}_o} = a q_e^2 \mathcal{E}_o$. Moreover, let us note that in the second term in (3.41) we can interchange both summations maintaining the condition $l \leq n$, viz

$$m_{\mathcal{E}_o} \sum_{l=1}^{N-1} \sigma_l^z \underbrace{\sum_{n=l}^{N-1}}_{(N-l)}. \tag{3.42}$$

Thus, the background field in (3.41) yields a position-dependent effective mass term for the spins in the chain, viz

$$\frac{m_{\mathcal{E}_o}}{2} \sum_{n=1}^{N-1} (N-n) \sigma_n^z.$$

The strength of this effective mass term in each site due to the background field is shown in figure 3.3.1

[1] Hereafter we are assuming open boundary conditions, but a straightforward modification of the final results yields an expression either for periodic or antiperiodic boundary conditions

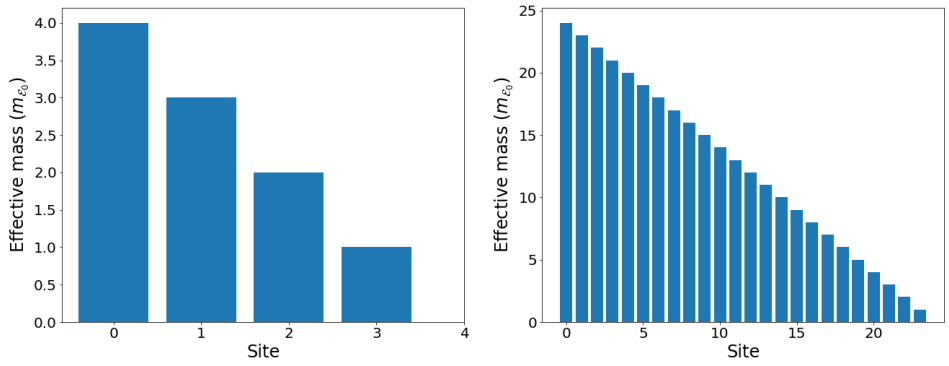

Figure 3.3.1: Plot of effective mass term due to the background field $\mathcal{E}_0$ for $N = 5$ and $N = 25$.

Now, let us simplify the first term in (3.41), to do so we use the equality

$$\xi \sum_{n=1}^{N-1} \frac{1}{4} \left(\sum_{l=1}^{n} \left[\sigma_l^z + (-1)^l \right] \right)^2$$
$$= \frac{\xi}{4} \sum_{n=1}^{N-1} \left(\sum_{l=1}^{n} \sum_{k=1}^{n} \sigma_l^z \sigma_k^z + 2 \underbrace{\sum_{l=1}^{n} (-1)^l}_{-n \mod 2} \sum_{k=1}^{n} \sigma_k^z + \sum_{l,k=1}^{n} (-1)^{l+k} \right), \tag{3.43}$$

coming from the standard form of the square of a summation. Note that the last term in (3.43) is a constant we can ignore. We have then the following

$$-\frac{m_\xi}{2} \sum_{n=1}^{N-1} (n \mod 2) \sum_{k=1}^{n} \sigma_k^z + \frac{\xi}{4} \sum_{n=1}^{N-1} \sum_{l=1}^{n} \sum_{k=1}^{n} \sigma_l^z \sigma_k^z, \tag{3.44}$$

with $m_\xi = q_e^2 a/2$. Note that again the first term of (3.43) is a position dependent effective fermion mass analogous to the one generated by the background field $\mathcal{E}_0$. The strength of the effective mass term, m_ξ, in each site is shown in figure 3.3.2.

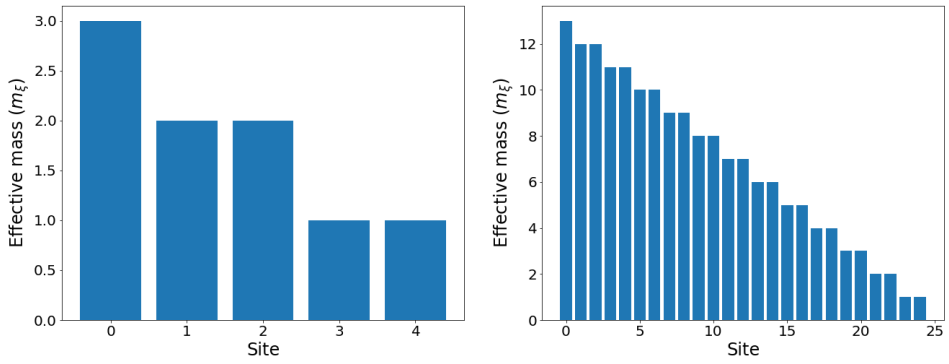

Figure 3.3.2: Plot of effective mass term, m_ξ, for $N = 5$ and $N = 25$.

Finally, let us focus our attention to the second term in (3.44). The two inner summations can be simplified by using the fact that $(\sigma^z)^2 = 1$, which yields a constant term we will ignore. And $[\sigma_l^z, \sigma_m^z] = 0$, implying that the crossed terms appear twice, viz

$$\frac{\xi}{4}\sum_{n=1}^{N-1}\sum_{l=1}^{n}\sum_{k=1}^{n}\sigma_l^z\sigma_k^z = \frac{\xi}{2}\sum_{n=1}^{N-1}\sum_{l=1}^{n}\sum_{k<l}\sigma_l^z\sigma_k^z. \tag{3.45}$$

Using the same interchange we used in (3.41), and enforcing the condition $l \leq n$ we obtain that

$$\frac{\xi}{2}\sum_{l=1}^{N-1}\sigma_l^z\underbrace{\sum_{n=l}^{N-1}}_{(N-l)}\sum_{k=1}^{l-1}\sigma_k^z, \tag{3.46}$$

interchanging the two summations one last time keeping in mind that $k < l$, we obtain the final expression for this term

$$J_{zz}\sum_{n=1}^{N-2}\sum_{m=n+1}^{N-1}(N-m)\sigma_n^z\sigma_m^z = J_{zz}\sum_{n<m}C_{nm}\sigma_n^z\sigma_m^z \tag{3.47}$$

with $J_{zz} = q_e^2 a/2$. We can plot the strength of the Coulomb C_{nm} interaction

in the lattice, this is shown in figure 3.3.3. This term is, as previously stated, long-range spin-spin interactions that are an effective description of Coulomb's law in our system.

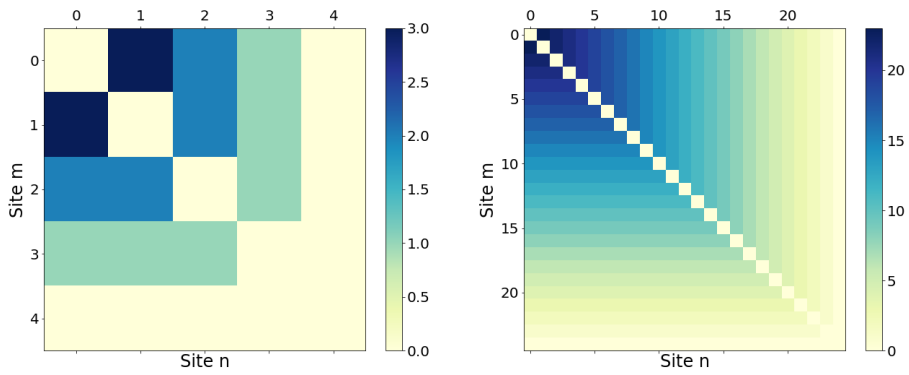

Figure 3.3.3: Plot of Coulomb strength interaction C_{nm} between spins in the lattice for $N = 5$ and $N = 25$.

After this calculation the Hamiltonian, which is expressed solely in terms of spin variables is

$$H = H_{p-a} + H_{\text{mass}} + H_{\text{eff. mass}} + H_{\text{Coulomb}} \tag{3.48}$$

such that

$$H_{p-a} = J \sum_{n=1}^{N-1} [\sigma_n^+ \sigma_{n+1}^- + \sigma_{n+1}^+ \sigma_n^-]$$

is a particle-antiparticle creation term.

$$H_{mass} = \frac{m}{2} \sum_n (-1)^n \sigma_n^z$$

is the fermion mass term.

$$H_{\text{eff. mass}} = \frac{m_{\mathcal{E}_0}}{2}\sum_{n=1}^{N-1}(N-n)\sigma_n^z - \frac{m_\xi}{2}\sum_{n=1}^{N-1}\sum_{k=1}^{n}(n \mod 2)\sigma_k^z$$
$$= \frac{m_{\mathcal{E}_0}}{2}\sum_{n=1}^{N-1} C_n\sigma_n^z - \frac{m_\xi}{2}\sum_{n=1}^{N-1} D_n\sigma_n^z$$

is the effective fermion masses term. And

$$H_{\text{Coulomb}} = J_{zz}\sum_{n<m} C_{nm}\sigma_n^z\sigma_m^z$$

is the Coulomb interaction between the spin in the lattice. It is very important to note that as a consequence of the restriction imposed by Gauss's law the physical Hilbert space of our lattice theory is the space of eigenstates of σ^z in each lattice site (with size 2^N), viz

$$\mathscr{H} = \bigotimes_{i=1}^{N} |s_i\rangle \tag{3.49}$$

3.4 Comment and conclusion

Throughout this chapter, we have explored the formulation and physics of the lattice Schwinger model. First in section 3.2, we described how a discretization of the continuum model could be made using Kogut-Susskind fermions. These fermions decompose the two-component two-dimensional spinor into a single component canonical fermion field in a staggered lattice, where the particles reside in the even lattice sites while the antiparticles are in the odd lattice sites. This decomposition avoids the *fermion doubling problem*, that is the appearance of various non-physical fermionic excitations as a consequence of a naive discretization of a continuum fermionic model [21]. With this in mind and having as a reference the analytic solution of the XY-model (cf. 2.2) we introduced a Jordan-Wigner transformation and showed the equivalence of the free lattice Schwinger model

with an XX spin chain. The equivalence to the XX-model without a transverse magnetic field in the case of $m = 0$, and with an XX-chain with a staggered transverse magnetic field in the case $m > 0$.

Subsequently, in subsection 3.2.2, we introduced the electric field into the lattice having as a guiding principle the method of gauge invariant point splitting to render the Lattice Hamiltonian gauge invariant. We showed that the lattice version of the electric field is realized by a quantum rotor residing in the links between the fermions (or spins). Having this result about the electric field it was easy to incorporate the background field into the formulation, as it boils down to adding the background field $\mathcal{E}_0$ to the electromagnetic Hamiltonian. We commented on how the discrete lattice model inherits the critical behavior of the continuum model. This behavior can be explored by studying the order parameters of axial fermion density Λ and of density of chiral condensate Γ.

Moreover, we showed the by imposing Gauss's law we can restrict the Hilbert space to the subspace of physical states and integrate out the gauge field degrees of freedom altogether from the lattice system. Hence, the Hamiltonian of the system is finally written solely in terms of the spin (or fermion content) of the lattice, namely

$$H = J\sum_n \left[\sigma_n^+\sigma_{n+1}^- + \text{h.c}\right] + \frac{m}{2}\sum_n (-1)^n\sigma_n^z + \xi\sum_n\left(\mathcal{E}_0 + \frac{1}{2}\sum_{l=1}^{n}\left[\sigma_l^z + (-1)^l\right]\right)^2.$$

Finally, in section 3.3, we showed that the electromagnetic term in the Hamiltonian of the lattice model, after imposing Gauss's law, gives rise to three non-trivial interaction terms in the system. First, it gives rise to an effective mass term which depends on the position of the spin within the chain. Secondly, it generates another effective

mass term appears due to the presence Background field $\mathcal{E}_o$. Both this contributions generate the following net effective mass Hamiltonian

$$H_{\text{eff. mass}} = \frac{m_{\mathcal{E}_o}}{2} \sum_{n=1}^{N-1} C_n \sigma_n^z - \frac{m_\xi}{2} \sum_{n=1}^{N-1} D_n \sigma_n^z.$$

The magnitude of the effective mass C_n and D_n are plotted in figures 3.3.1 and 3.3.2 respectively. Lastly, another term arising from the electromagnetic Hamiltonian is a spin-spin interaction which is linear in distance, being an effective description of Coulomb's interaction in the system. This term is described by the Hamiltonian

$$H_{\text{Coulomb}} = J_{zz} \sum_{n<m} C_{nm} \sigma_n^z \sigma_m^z,$$

where the strength of the coupling C_{nm} is plotted in figure 3.3.3. This term of spin-spin interaction breaks the integrability of the lattice system and forces us to abandon the hope of solving the system analytically. Rather, we must appeal to numerical simulation in order to study the dynamics and physically relevant quantities of the system. This endeavor will be presented in the next chapter.

4

Simulations of the Schwinger model

4.1 Motivations and introduction

As commented in previous chapters the Schwinger model is a very interesting gauge theory which due to its simplicity is ideal for the methods of lattice gauge theory. And as such, we take advantage of a discrete version of the model in order to simulate it on a discrete lattice in a computer. This is useful as many physical characteristics of the continuum model can be studied using lattice simulations.

In this chapter we present simulations for three distinct models: The free massless model, the free massive model, and the fully interacting model, both massless and massive. Using a python package designed for exact diagonalization of discrete fermion or spin systems, we study the relevant physical quantities of the models such as their spectrum, their ground state energy density and the order parameters

for the case of the interacting model.

Additionally, there has been a recent and strong interest in non-equilibrium phenomena in quantum many-body systems sparked primarily by the advancement of experimental techniques in quantum control and simulation of many-body dynamics of interacting quantum systems. Experimental realizations of Bose-Einstein condensates and cold atomic gases trapped in optical lattices permit the precise experimental study of many-body interacting dynamics The careful control of the system parameters makes this a rich ground to explore the system's non-equilibrium dynamics. As a theoretical motivation one can take as a guiding principle the way that statistical mechanics of equilibrium systems describes emergent phenomena as the result of the microscopic dynamics of the atoms in a physical system. In the context of equilibrium statistical mechanics very important notions such as work, entropy and phase transitions emerge and are of great physical interest. Hence, an important question comes to mind when thinking about the non-equilibrium dynamics of quantum systems: what physically relevant properties of the system under study can we obtain from a careful study of its non-equilibrium dynamics?

Thus, in light of the previous motivation we are interested in studying some out of equilibrium properties of the interacting Schwinger model which can be simulated in a computer with python. In the last section of this chapter, we simulate and study simple quantum quench dynamics of the interacting model for various background fields. We are interested in some of its out of equilibrium properties, in particular we want to study the behavior of the axial fermion density and the chiral condensate density, which are order parameters of the system, whenever a global quench in the background field is introduced in the model.

4.2 A comment on exact diagonalization

The method used in this thesis to obtain the energy levels of the Hamiltonian of the lattice system is exact diagonalization. This is done by using Quspin [25, 26],

a python package for exact diagonalization of fermion and spin chains. The aim of the exact diagonalization method is to construct the full Hamiltonian of the lattice model and compute its spectrum which needs to be finite. This first step toward the exact diagonalization of a system is to construct a basis of the Hilbert space describing the system. Since we are dealing with spin systems, or equivalently fermion chain in one dimension, all possible many-body states are constructed by taking either a spin up $|\uparrow\rangle$ or spin down $|\downarrow\rangle$ states (filled $|1\rangle$ or empty site $|0\rangle$ in the case of fermions) in each site of the lattice. Thus, we have two possible states for each lattice site for a total of 2^N possible states which of course is the size of the basis. After fixing the basis we construct a representation of the Hamiltonian of the system on this basis

$$H_{ij} = \left\langle \psi_i \right| H \left| \psi_j \right\rangle \tag{4.1}$$

which turns out to be a $2^N \times 2^N$ matrix which in most cases is very sparse. The diagonalization is made invoking the ARPACK package which is designed to compute a few eigenvalues and corresponding eigenvectors of a large sparse matrix, using a combination of Arnoldi and Lanczos processes [27]. The biggest drawback of the exact diagonalization method is a memory problem as the number of states grows exponentially with the system size. However, for our purposes, the method will be very useful.

4.3 The free massless Schwinger model

The first model we will explore will be the massless Schwinger model in absence of electromagnetic field, i.e. an XX-model with zero transverse magnetic field. The Hamiltonian we will simulate is 2.23 for $N \in [4, 24]$. To obtain the energy levels and the spectrum of the Hamiltonian we use exact diagonalization by using the python package Quspin. We plot the spectrum of the free Hamiltonian in real space in figure 4.3.1 (left panel). Here we take batches of 8 eigenvalues in order to show the structure of the spectrum and avoid clutter in the plot.

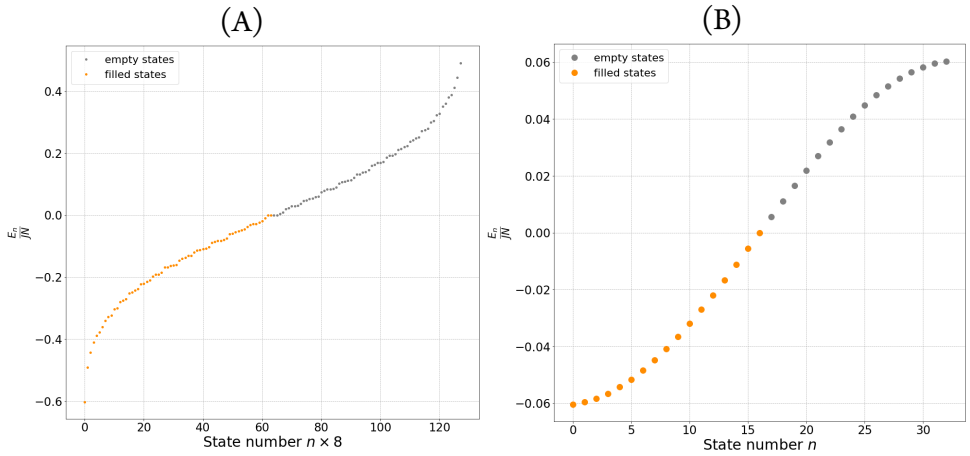

Figure 4.3.1: Full spectrum of the Hamiltonian in real space. (A) Spectrum for $N = 14$ taking batches of 8 eigenvalues to show the spectrum structure and avoid clutter. (B) Single particle excitation spectrum for $N = 33$.

In figure 4.3.1 the orange dots are the filled states of the Dirac sea with negative energy, while the gray ones correspond to empty states above the Fermi level with positive energy (cf. 2.3).

Similarly, we can plot the single particle excitation spectrum for a longer chain shown in figure 4.3.1 (right panel). This is possible as the system is non-interacting and the many-body wave function factorizes in a product of single-particle states. This decomposition has the advantage of avoiding the exponential scaling of the Hilbert space dimension by simulating the dynamics of a single particle. As we see the single-particle excitation spectrum is qualitatively very similar to the spectrum of the XX-model without a transverse field plotted in figure 2.3.1.

Moreover, we simulate the free Schwinger model from $N = 4$ up to $N = 24$ having as an objective to compute the smallest eigenvalue of the Hamiltonian, which corresponds to the ground state energy. Having the smallest eigenvalue we can compute the energy density for each lattice size, which we see from figure 4.3.2 approaches the thermodynamic limit value $-1/\pi$. Hence the free massless model corresponds with an XX spin chain without a transverse magnetic field.

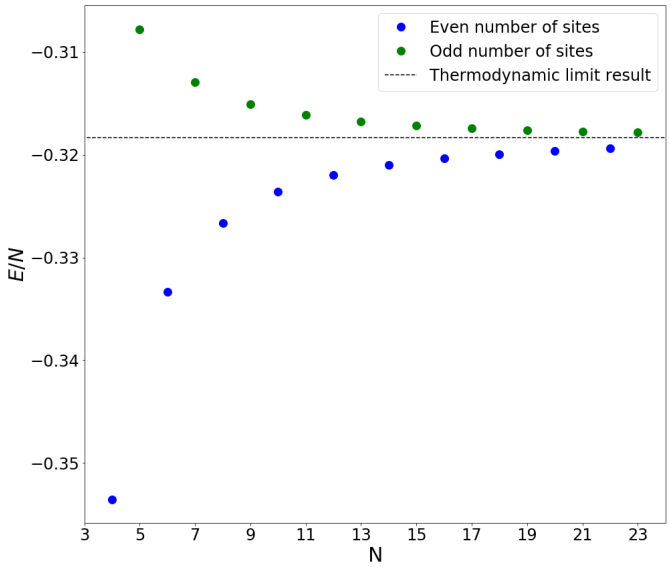

Figure 4.3.2: Ground state energy per site for $N \in [4, 24]$ for even and odd number of particles. The dashed black line is the result in the thermodynamic limit where $E_0/N = -1/\pi$

Additionally, in figure 4.3.3 we show the energy densities of the first three excited states of the system for various lattice sizes. From the plots, we see how the all the states approach rapidly the thermodynamic energy density $-1/\pi \approx -0.318309$. To make this idea precise, note that the energy density for one dimensional free systems should scale roughly as the particle in a box energy density

$$\frac{E_0}{N} \sim \frac{1}{N^2}.$$

Hence, if we plot the energy density of our model against N^{-2} and make a linear fit to the simulation data, we can extract the value of the energy density in the thermodynamic limit. The linear fits are shown in 4.3.3. It is also crucial to note, that from these plots we can infer that there is no energy gap between the ground state and the first excited states for the free massless lattice Schwinger model in the

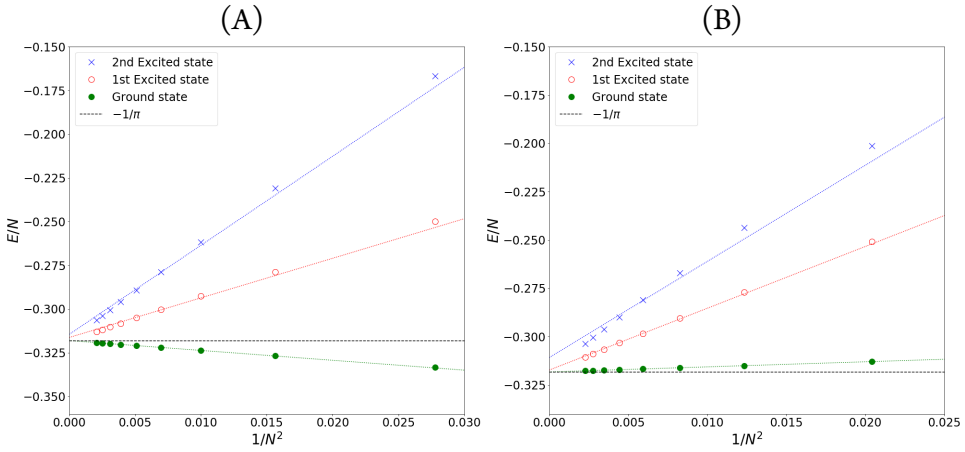

Figure 4.3.3: Plot of the ground state and the first two excited states energy densities versus the inverse of the number of sites squared with $N \in [4, 22]$. Normalization of the energy density with m is made to preserve the y scale. (A) Even number of particles. (B) Odd number of particles. A linear fit is made to determine numerically the ground state energy

thermodynamic limit. This is clear as all the three linear fits are converging towards $-1/\pi$ in the limit of $N \to \infty$ in figure 4.3.3. We can determine numerically the intercept of the best fit lines to extrapolate the thermodynamic value, doing this gives us the following results

$$\frac{E_0}{N} = -0.31797, \quad \text{N even}\,; \qquad \frac{E_0}{N} = -0.31832, \quad \text{N odd}. \tag{4.2}$$

Thus, the numerical result extracted from our simulations is precise to within a part in one thousand compared to the thermodynamic limit energy density for the XX-model result, which is very very close.

4.4 The free massive Schwinger model

The second model we will explore is the massive Schwinger model in absence of electromagnetic field but with non-zero mass, i.e. an XX-model with a traverse staggered magnetic filed. The Hamiltonian we will simulate is 3.13. To obtain the energy levels and the spectrum of the Hamiltonian we use the exact diagonalization

method in Quspin. First, we plot the full spectrum in real space for different mass values in figure 4.4.1. This is done to study how varying the fermion mass affects the eigenvalue structure. In figure 4.4.1 the energy of each state E_n is normalized with the mass in order to fix the y scale of the plots.

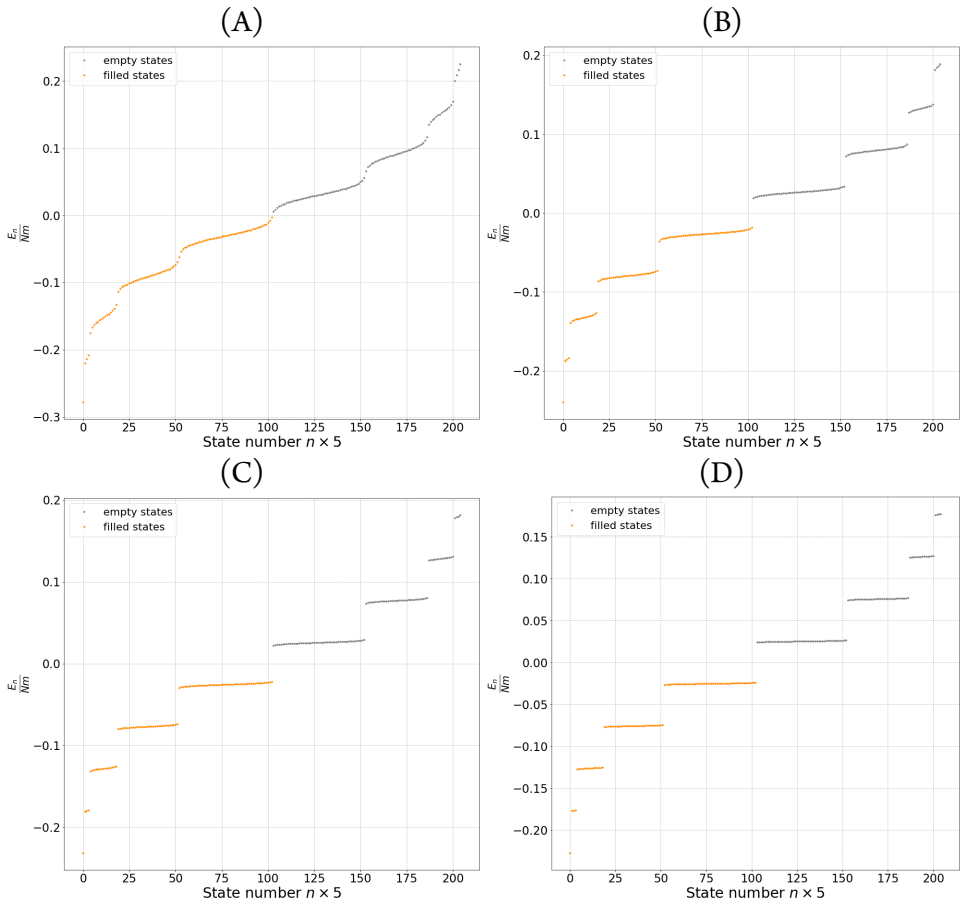

Figure 4.4.1: Plot of the spectrum in real space for different values of the mass taking batches of 5 eigenvalues. (A) $m = 2$, (B) $m = 4$, (C) $m = 6$ and (D) $m = 10$.

A close examination of figure 4.4.1 reveals a very interesting evolution of the spectrum with increasing mass. Note that as the mass parameter increases, the spectrum acquires a ladder-like structure, forming separate eigenvalue manifolds

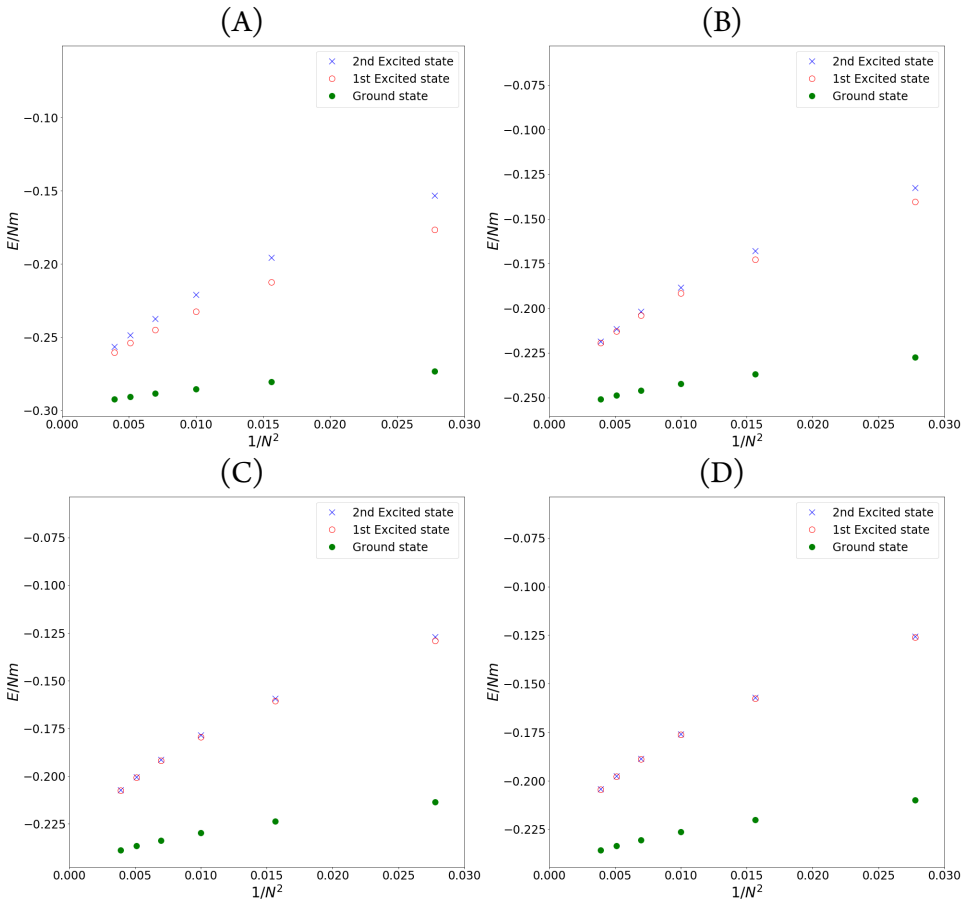

Figure 4.4.2: Plot of the ground state and the first two excited states energy densities versus the inverse of the number of sites squared with $N \in [4, 18]$ and N even. Normalization of the energy density with m is made to preserve the y scale. (A) $m = 2$, (B) $m = 4$, (C) $m = 6$ and (D) $m = 12$.

having roughly the same energy. Making the interpretation of this degeneracy rather simple, As the ratio J/m decreases the Hamiltonian is dominated by a simple transverse field term (cf. 2.2)

$$H \sim \sum_n (-1)^n \sigma_n^z, \tag{4.3}$$

thus, in the limit of a very large mass, like the case of $m = 10$ in figure 4.4.1, the Hamiltonian of the system is for all intents and purposes is 4.3. Therefore, each separate manifold corresponds to a particular configuration of the spins (either aligned or anti-aligned with the z axis) in the chain yielding a specific energy of this Hamiltonian. In particular, we observe that the single lowest energy state, i.e the ground state, is non-degenerate which means there exists a single spin configuration which minimizes the energy. This state corresponds to all the spin located on even sites being in $|\downarrow\rangle$ state, while the spins on odd lattice sites being in $|\uparrow\rangle$ state. A similar analysis can be made for the most energetic state, where all the spin located on odd sites are in the $|\downarrow\rangle$ state, while the spins on even lattice sites are in the $|\uparrow\rangle$ state . As to the degenerate eigenvalue manifolds in the spectrum, they can be understood as follows, several spin configuration yield the same energy, since permuting spins in different sites with the same configuration does not affect the valu of the energy. This fact accounts for the ladder-like structure of the spectrum, i.e this manifolds are invariant under a fixed number of permutations of the spins with the same state with respect to (4.3). This degeneracy is exact in the limit of very large mass $m \to \infty$, where the particle-antiparticle term of the Hamiltonian can be disregarded. Nevertheless, even though the effect of this term in small whenever $J/m < 0.2$ it is not negligible as it "bends" the ends of each of the eigenvalue manifolds towards the closest manifold. Note that this bending effect is clear from the evolution of the spectrum as the mass parameter decreases. In the top left panel of figure 4.4.1, we see how the manifolds start to form and "rotate", separating from each other. In the top right panel, we can clearly differentiate each manifold, but we note that they are not fully degenerate in energy due to the particle-antiparticle term of the Hamiltonian. However, when the mass term

becomes relevant compared to the value of J, as we see in the lower panel, the manifolds separate sharply and become increasingly degenerate.

Of particular interest to us is the structure of the ground state and the first excited states of the system, especially whether there exists of an energy gap between the ground state and the first excited state. To this end, we show in figure 4.4.2 a plot of the energy density as a function of the inverse of the number of sites squared for an even number of sites taking different fermion massess [1].

From figure 4.4.2 we can conclude two important facts, First and foremost, there is an appreciable energy gap, Δ_E, present as the first excited state energy density, plotted as a hollow red circles in figure 4.4.2, in the limit $n \to \infty$ clearly will not converge to the ground state energy density, shown as filled green circles. Secondly, as the ratio J/m decreases the appearance of the eigenvalue manifold degeneration becomes evident even for the first and second excited states. Namely, as the mass parameter increases as we see in 4.4.2 (C) and (D) the first and second excited states overlap, effectively demonstrating the ladder-like structure of the spectrum which is becoming increasingly degenerate as mass increases.

Finally, let us comment on the appearance of the energy gap in the massive model. Analytically, we can define the energy gap for the single particle spectrum of the XX-model (cf. section 2.3) as

$$\Delta_E \doteq \varepsilon_{k=0} = (g - J). \tag{4.4}$$

Recall that in the case of the free massive lattice Schwinger model, $m/2$ is equivalent to the staggered transverse magnetic field g in the XX-model (cf. section 3.2). To make this precise, note that the energy gap should be linear on the mass and it should be shifted from zero by an amount J. In figure 4.4.3 we show a plot of the

[1] The plots for odd number of sites show essentially the same behavior and thus are not particularly more illuminating.

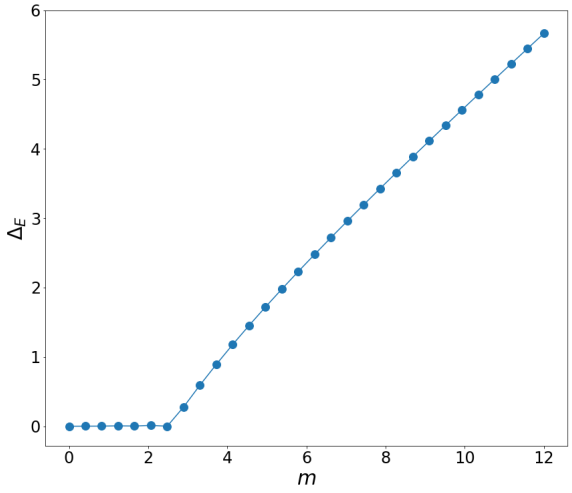

Figure 4.4.3: Spectrum gap energy as a function of mass

energy gap resulting from simulations of systems with varying masses in the range $m \in [0, 12]$. We see from this figure what we anticipated previously from studying the XX-model. The energy gap is indeed linear in mass and is shifted from zero by J as expected. This confirms the equivalence between the free massive Schwinger model and the XX-model in the presence of a transverse staggered magnetic field.

4.5 The interacting Schwinger Model

Finally, the third model we will explore is the fully interacting Schwinger model (either massless or with non-zero mass). As a first simulation, we are interested in studying the energy density of the ground state for the massless interacting model. To do this we simulate the model varying the fermion charge q_e. We expect that whenever q_e approaches zero the energy density of the ground state tends to $-1/\pi$ as the model becomes free.

Results of this simulation are shown in figure 4.5.1. We see that whenever the

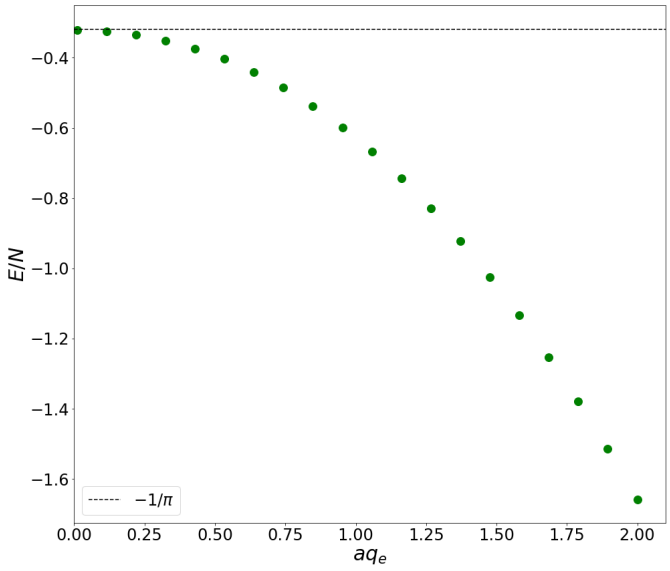

Figure 4.5.1: Plot of the ground state energy density for the massless interacting Schwinger model.

electron charge tends to zero the value of the energy density tends to the value of the free model as we should expect. Additionally, we see that for increasing values of q_e the ground state energy per spin increases as the Hamiltonian is dominated by the electromagnetic energy stored in the electric field.

Additionally, beyond the ground state, we are interested in studying the behavior of the order parameters of the system. These parameters are the density of chiral condensate Γ and the axial fermion density Λ. We have simulated a system of $N = 14$ spins for $m \in \{0.0, 2.0\}$. and different values of the background electric field $\mathcal{E}_0$. Let us discuss briefly the results for each order parameter separately.

First, in figure 4.5.2 we observe the results of chiral condensate density of simulating systems with varying fermion charge. Note that we have selected values greater and smaller than the critical value of $\mathcal{E}_0 = 0.5$ where the phase transition occurs. Additionally observe that the value $\mathcal{E}_0 = 0.5$ sharply separates the regions $\mathcal{E}_0 >$

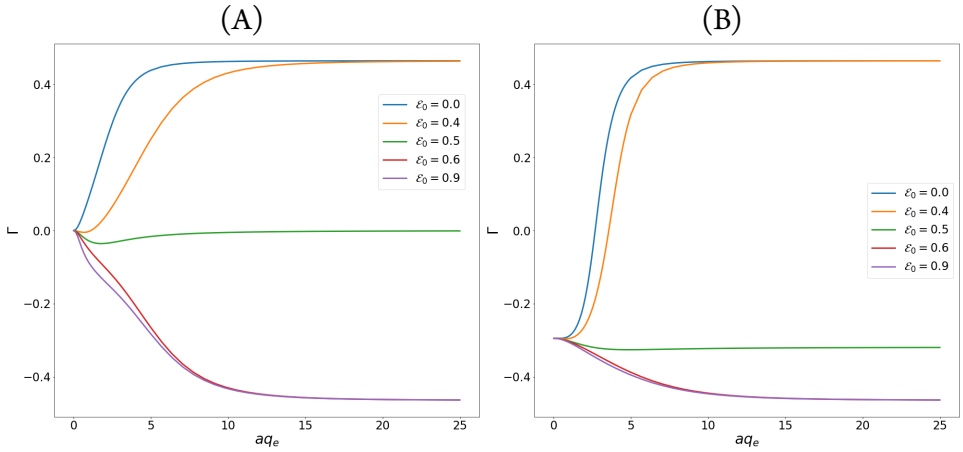

Figure 4.5.2: Plot of the density of chiral condensate as a function of q_e, $q_e \in [0, 25]$. (A) Massless case $m = 0$. (B) Massive Case $m = 2.0$.

0.5 and $\mathcal{E}_0 < 0.5$. We see that in both this regions as fermion charge increases the values of Γ approach the approximate values $\Gamma \approx \pm 0.45$. This means that there are two distinct field configurations separated by $\mathcal{E}_0 = 0.5$. Recall, that in the first chapter we have discussed how the energetics of pair production in one-dimensional space gives rise to this critical behavior (cf section 1.2.1). The appearance of two separate regions we observe in figure 4.5.2 is a reflection of the dynamics a particle-antiparticle production due to the background field. Finally, note that the behavior for the massive case roughly the same as the massless one. The only difference is that whenever $q_e \to 0$ in the massive case, $\Gamma \neq 0$. Therefore, we can conclude that the presence of mass fixes a non-zero value of the chiral condensate. This can be understood by noting that the mass Hamiltonian

$$H_{\text{mass}} \sim \sum \sigma^z,$$

being proportional to σ^z is clearly relevant for the value of Γ (cf. section 3.2). However, the reader might ask what about the effective mass terms introduced the presence: of the electric field? Don't they also contribute to Γ? The answers to these questions are straightforward. Note that from the plots of the effective mass coupling (cf. figures 3.3.1 and 3.3.2) we can see their relative strength is basically

equal, however, they appear in the Hamiltonian with opposite signs therefore, their contributions to Γ gets canceled and the net effect is rather small.

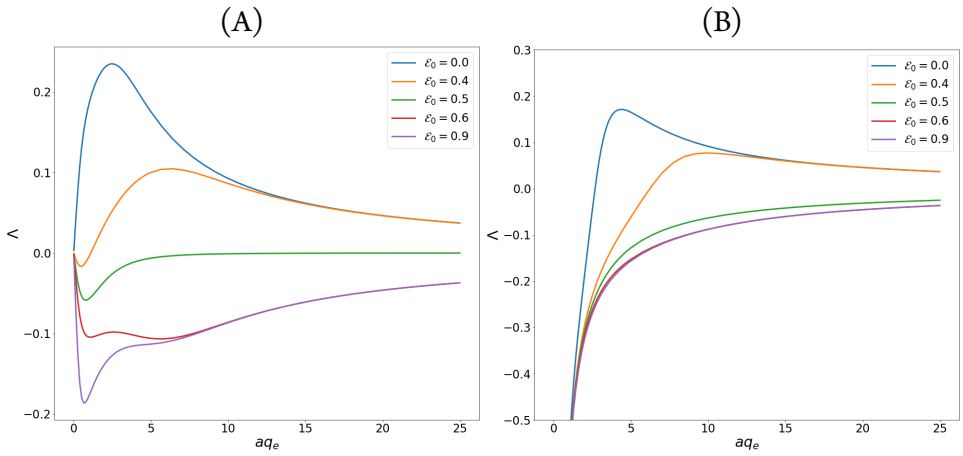

Figure 4.5.3: Plot of the axial fermion density as a function of q_e, $q_e \in [0, 25]$ for different background field values. (A) Massless case $m = 0$. (B) Massive Case $m = 2.0$.

Second, in figure 4.5.3 we observe the results from the axial fermion density obtained by simulating systems with varying fermion charge. We see that in the case $m = 0.0$, there is a behavior similar to the one described for the density of chiral condensate. There are two distinct values where the curves for Λ overlap as q_e increases. Nevertheless, the plot for $m = 2.0$ shows a very different result. In this case, we see that the curves for Λ for all values of $\mathcal{E}_0$ overlap and very rapidly tend towards zero. This can be understood by noting that Λ is essentially the particle-antiparticle portion of the Hamiltonian (cf. section 3.2) and thus as the background field increases the phenomenon of pair production begins in the system in order to screen the background field. However, as soon as massive particle-antiparticle pairs are created from vacuum dielectric breakdown, the expectation value of the axial fermion density tends to vanish. Nevertheless, as opposed to the massless case, in the massive case the production of a particle anti-particle pair from vacuum costs at least twice the rest mass of the particle. Therefore, these pairs

are rapidly created to screen the background field until it is no longer energetically favorable for the vacuum to create any more pairs and the axial density rapidly vanishes.

Moreover, the relationship between Γ and Λ with mass was studied for $\mathcal{E}_0 = 0.0, 0.5, 0.9$ and $m \in [0, 1]$. The results are shown in figure 4.5.4. We can see from the plots that for increasing m both Λ and Γ curves overlap and tend to a fixed value. In the case of Λ, we see a steady decrease towards 0 which means that the axial fermion density vanishes for $m \neq 0$. This is consistent with was commented before in reference to figure 4.5.3.

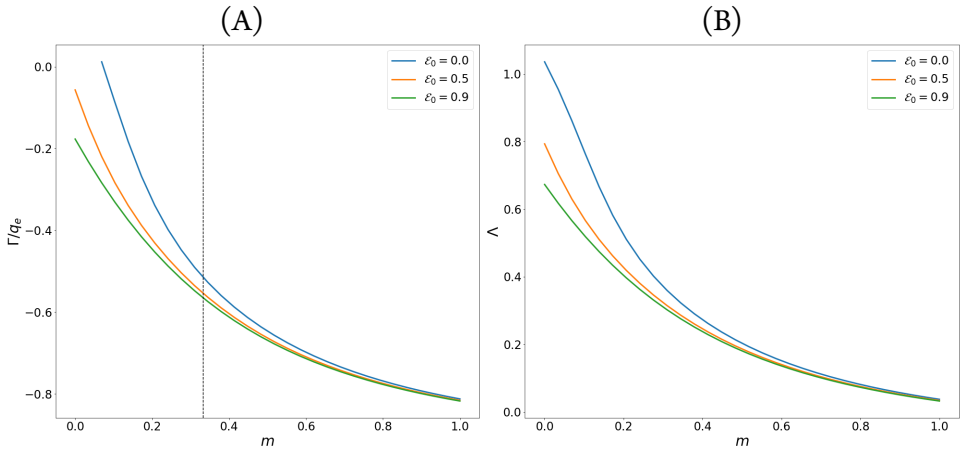

Figure 4.5.4: Plot of the order parameters as a function of fermion mass $m \in [0, 1]$ for different background field values.The fermion charge q_e is set to 1. (A) Γ/q_e as a function of m. Dotted line at $m/g = 0.3$ for reference. (B) Λ as a function of m.

Additionally, we can say qualitatively that from the form of Γ at $\mathcal{E}_0$ there is a phase transition at a value close to $m/q_e = 0.3$. Above $\mathcal{E}_0 = 0.5$ the chiral symmetry of the theory is broken due to the background field and there are two degenerate vacuum states [5, 24]. Note the different behavior for $\mathcal{E}_0 = 0.0$ and for $\mathcal{E}_0 = 0.9$, where roughly at $m/q_e = 0.3$ the curves diverge approaching

$\Gamma/q_e \approx \pm 0.2$ at vanishing mass.

4.6 Quantum quenches in the Schwinger model

The study of closed quantum systems out of equilibrium is of the utmost importance in order to understand the dynamics of nature out of the equilibrium regime. Non-equilibrium processes are readily present in most areas of physics, therefore, a better understanding of non-equilibrium phenomena is paramount to a broader understanding of nature and its nuances. Nonetheless, such ventures out of equilibrium are in general very hard problems to tackle, and solutions are often absent. The question is then: how can we study the out of equilibrium dynamics of quantum systems in a way that gives illustrative answers?

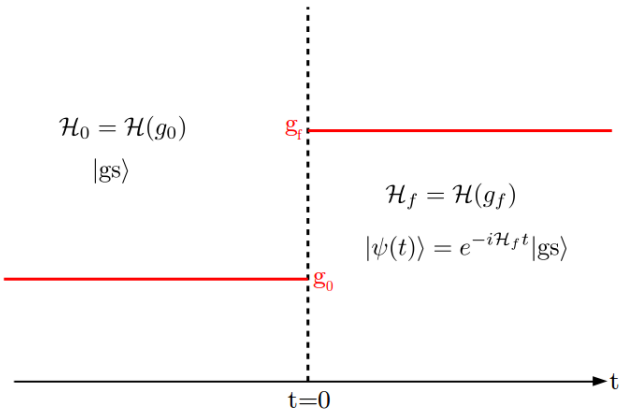

Figure 4.6.1: Quantum quench protocol.

There is a very large number of ways of driving quantum systems out of equilibrium, and most of them turn the exact calculation of system dynamics into a formidable and often impossible task. Therefore, the name of the game is to find a way to "kick" the system out of equilibrium in a way that enables calculation of the most relevant system properties. One of the most popular ways to "kick" a system out of equilibrium is known as a *quantum quench* . The idea behind a quantum quench

is to prepare the system in a non-equilibrium state whose evolution is dictated in terms of the system's Hamiltonian. This implies in particular, preparing the system in the ground state $|\mathrm{GS}\rangle$ of a Hamiltonian H_0 and subsequently, evolving the state unitarily according to a different Hamiltonian H_1

$$|\psi(t)\rangle = e^{-itH_1}\,|\mathrm{GS}\rangle\,; \quad t > 0, \quad [H_0, H_1] \neq 0$$

Hereafter, let $H(g)$ be the system Hamiltonian dependent on some external parameter g, that can be, for example, an electric or magnetic field or the interaction strength between particles. In a *global quantum quench* $H_0 = H(g_0)$ at some given initial value of the external parameter and at a fixed time, say $t = 0$ a sudden switch in the Hamiltonian parameters occurs, $H_1 = H(g_f)$ where g_f is a new value of the parameter. Thus, the quenching protocol of interest to us consists of changes in Hamiltonian parameters of a given system (see figure 4.6.1). There are also other popular quenching protocols: *local quenches* where the quench is limited to a bounded regions of the system; *sweeps* where the change in parameter has an explicit time dependence given some detailed protocol; and *geometric quenches* where the spatial configuration of the system is changed, for example, a sudden change from periodic to open boundary conditions.

The objective of a quench is to study the evolution of observables that can give physical insight into the dynamics of the system, viz

$$\langle \mathcal{O}_1 \cdot \mathcal{O}_2 \cdot \ldots \cdot \mathcal{O}_n \rangle\,(t) = \frac{\langle \psi(t)|\mathcal{O}_1 \cdot \mathcal{O}_2 \cdot \ldots \cdot \mathcal{O}_n|\psi(t)\rangle}{\langle \psi(t)|\psi(t)\rangle} \tag{4.5}$$

where each $\mathcal{O}_i$ is a local observable. Assuming that H_1 has a discrete spectrum $\{E_n\}$ and recalling that our time evolved state $\psi(t)$ can be written in terms of our pre-quench ground state we can rewrite any expected value of a local operator $\mathcal{O}(t)$ as

$$\langle \mathcal{O} \rangle\,(t) = \sum_{m,n} \langle \mathrm{GS}|E_m\rangle\,\langle E_n|\mathrm{GS}\rangle\;\langle E_m|\mathcal{O}|E_n\rangle\,e^{-i(E_m - E_n)t}. \tag{4.6}$$

Another important quantity in the study of quantum quenches is the Loschmidt

amplitude

$$\mathcal{L}(t) = \langle GS|e^{iH_0 t}e^{-iH_f t}|GS\rangle = \langle GS|e^{-iH_f t}|GS\rangle\,, \tag{4.7}$$

since $|GS\rangle$ is the ground state of H_0 the last equality follows from the fact that $H_0|GS\rangle = 0$. This amplitude quantifies how far from equilibrium a system is taken due to the evolution generated by Hamiltonian dynamics. Additionally, we can compute form the Loschmidt amplitude its modulus squared

$$L(t) = |\mathcal{L}(t)|^2, \tag{4.8}$$

known as the Loschmidt echo. This quantity gives a measure of the stability of the system dynamics along time evolution.

Thus, in a quantum quench one addresses several important aspects related to the dynamics of our system, namely:

- **Thermodynamics:** Due to the sudden change in the systems Hamiltonian work is done to the system and its internal energy is abruptly altered. This sudden change generates a real-time evolution between equilibrium states of H_0 and H_1.
- **Real-time dynamics and relaxation:** As a consequence of the abrupt perturbation the system has to adjust and relax to an equilibrium state. The time scales and asymptotic behavior of such a process may give relevant physical information of our system.
- **Thermalization** Classically a system that is taken out equilibrium evolves to an equilibrium configuration after a sufficiently long time scale. On the context of quantum quench dynamics, an important question that has not been definitely answered is whether a closed quenched quantum system prepared in a non-equilibrium state can reach an equilibrium configuration without a coupling to an environment.

4.6.1 Quenches from the free model

The first type of quantum quench we will explore will be a quench starting from the free massless Schwinger model to the interacting massless Schwinger model. Therefore, for this particular quench, we take the initial Hamiltonian H_0 to be the Hamiltonian for the free massless model, i.e. the XX-model Hamiltonian with its corresponding ground state $|GS\rangle$. The final Hamiltonians H_f, post quenching will be the Hamiltonian of the interacting massless Schwinger with background field for $\mathcal{E}_0 = 0.0$ and $\mathcal{E}_0 = 0.5$. For this quench, we will study two quantities that interesting in this context, First, we will study the Loschmidt echo density

$$\frac{|\mathcal{L}(t)|^2}{L} = \frac{L(t)}{L}. \tag{4.9}$$

we call it a density as it is divided by the number of lattice sites. Second, we will study the expectation value of the density of chiral condensate between the ground state of the initial Hamiltonian and the time evolved state generated by the interacting Hamiltonian, viz

$$\tilde{\Gamma}(t) \doteq \langle GS|\Gamma e^{-iH_f t}|GS\rangle\,, \tag{4.10}$$

and the same expectation value for the axial fermion density

$$\tilde{\Lambda}(t) \doteq \langle GS|\Lambda e^{-iH_f t}|GS\rangle\,. \tag{4.11}$$

Results for the Loschmidt echo density are shown in figure 4.6.2.

In figure 4.6.2 we can see the oscillatory behavior of the Loschmidt for both values of the background field. Both plots have a similar oscillation frequency, however, see that clearly, the oscillation amplitude is greater for the quench to the interacting model with $\mathcal{E}_0 = 0.0$.

The results for the chiral condensate density are shown in figure 4.6.3. In this plot, we see how the expectation value of Γ oscillates in both cases with roughly

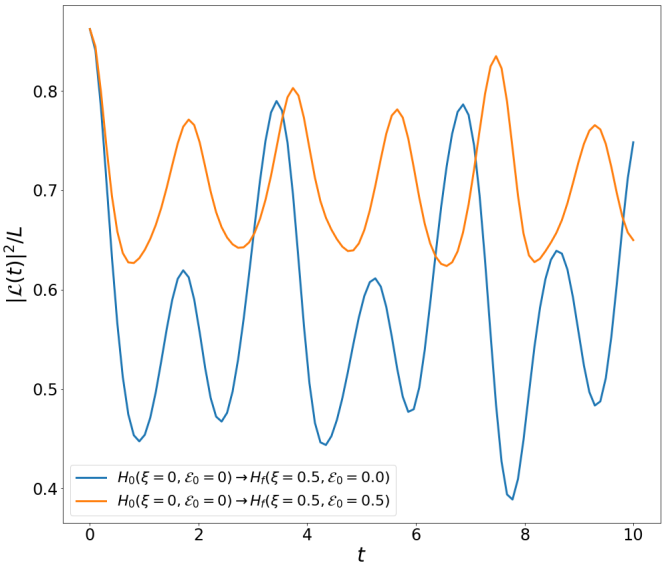

Figure 4.6.2: Plot of the Loschmidt echo density as a function of time for a quench from the free model to the interacting model. Blue line corresponds to $\mathcal{E}_0 = 0.0$. Yellow line corresponds to $\mathcal{E}_0 = 0.5$.

the same frequency, but again as mentioned earlier, the plot for zero background field has a greater amplitude than the case of a non-zero background field.

4.6.2 Quenches between background fields

Finally, the second type of quantum quench we are interested in is one which the initial Hamiltonian is the massless interacting Hamiltonian without background electric field to the Hamiltonian corresponding to the massless interacting model with a background field $\mathcal{E}_0 = 0.5$. In figure 4.6.4 we can see how the Loschmidt echo density evolves with time. Note that, the time evolution is given by an oscillatory function resembling a cosine function. Hence, we can say that the dynamics of the interacting model is oscillatory whenever the background field changes abruptly. This makes sense if we note that if the background field is suddenly switched on it will induce dielectric breakdown from the vacuum followed shortly by pair production. This will screen the electric field effectively reducing its value below the critical one

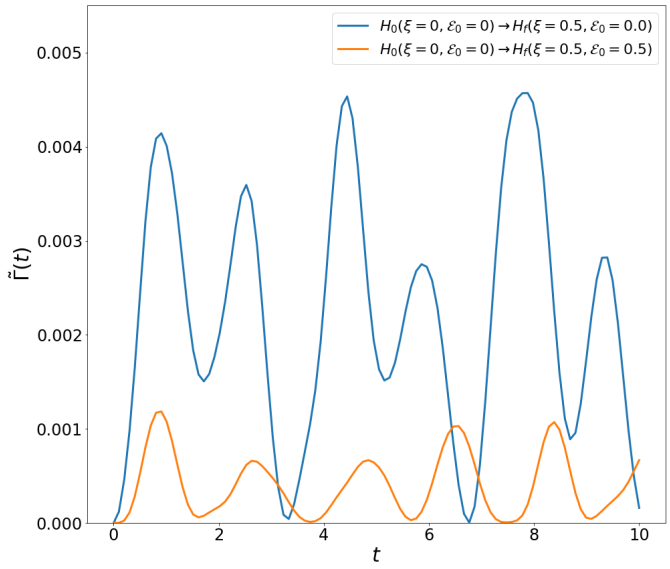

Figure 4.6.3: Plot of the density of chiral condensate as a function of time for a quench from the free model to the interacting model. Blue line corresponds to $\mathcal{E}_0 = 0.0$. Yellow line corresponds to $\mathcal{E}_0 = 0.5$.

(cf. subsection 1.2.1).

Finally, in figure 4.6.5 we see the time evolution of the two order parameters characterizing the critical behavior induced by the background filed. Note that both plots show an oscillating behavior which can be understood roughly in the same manner as we previously commented for the Loschmidt echo density. However, we see that the axial fermion density oscillates somewhat more randomly compared to the chiral condensate density. This can be traced back yet again, to the dynamics of pair-production induced by the background field, recall that the axial fermion density operator is essentially a particle-antiparticle creation-annihilation operator. Hence, it is very sensitive to the presence of particle-antiparticle pairs, and we expect it to oscillate more rapidly. Furthermore, observe that the dynamics of the density of chiral condensate are roughly the same as the ones we found from the quench between the free and interacting model. Nonetheless, the sharp oscillatory behavior of Γ indicates to us that a quench from an eigenstate of the interacting

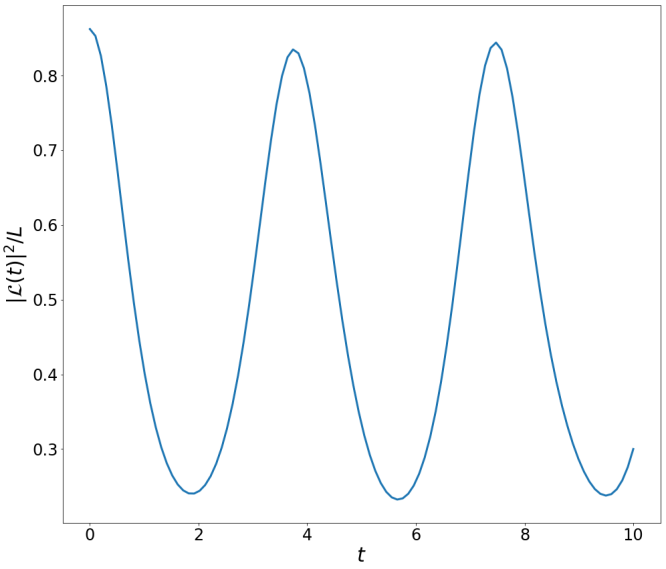

Figure 4.6.4: Plot of the Loschmidt echo density as a function of time for a quantum quench between the massless interacting Hamiltonian with $\mathcal{E}_0 = 0.0$ to the massless interacting Hamiltonian with $\mathcal{E}_0 = 0.5$.

model with $\mathcal{E}_0 = 0.0$ to an eigenstate of the interacting model with $\mathcal{E}_0 = 0.5$ is taking the system out of equilibrium. Moreover, besides taking the system out of equilibrium the quench is crossing a point where a phase transition occurs (cf subsection 1.2.1) which fundamentally drives the system out of equilibrium and explains the abrupt changes and oscillatory behavior of the order parameters of the system.

4.7 Comments and conclusion

Throughout this chapter, we have numerically studied the lattice Schwinger model in all of its variants, i.e. the free massless Schwinger model, the free massive Schwinger model and the massless & massive interacting model with and without a background electric field. We have used the exact diagonalization methods in order to simulate and study lattice models with a small number of degrees of freedom. To this end,

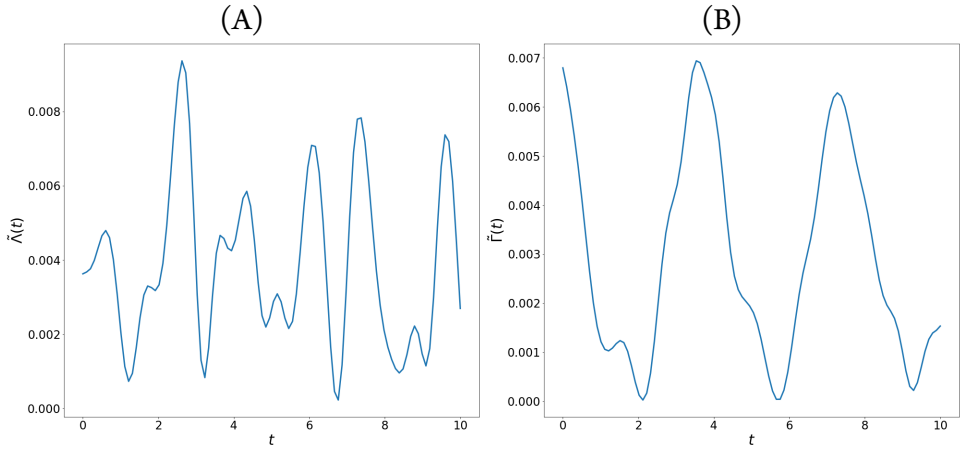

Figure 4.6.5: Plot of the order parameters as a function of time for a quantum quench between the massless interacting Hamiltonian with $\mathcal{E}_0 = 0.0$ to the massless interacting Hamiltonian with $\mathcal{E}_0 = 0.5$. (A) Axial fermion density. (B) Density of chiral condensate.

we employed the python package *Quspin*, to facilitate the numerical computations. For the free massless model, we computed its spectrum in real space and the single particle spectrum and commented on the structure of the half-filled band. Moreover, we showed, by simulating systems with increasing size, that the vacuum energy density in the limit of an infinite number of lattice sites tends to the value $-1/\pi$. This value is the continuum limit energy density for the XX-model which we showed was equivalent to the free Schwinger model. For the free massive model, we also studied the spectrum for varying mass and commented on the appearance of distinct eigenvalue manifolds as a consequence of the degeneracy of the eigenstates of the mass Hamiltonian. We computed the ground state and the first excited states energy densities and commented on the appearance of a spectrum energy gap due to the mass term. And furthermore, we confirmed that the energy gap should be linear with mass.

With respect to the interacting model, we computed its ground state energy density and showed it reduces to the case of the free model whenever the mass is zero. Additionally, we computed the values of the axial fermion and chiral condensate

order parameters for various values of the background field. We observed that the value $\mathcal{E}_0 = 0.5$ is special since it separates the possible values of the order parameters in two distinct values at strong coupling. And we commented qualitatively how from the overall form of the chiral condensate density order parameter one can suspect the appearance of a critical behavior.

Finally, in the last section, we briefly introduced quantum quenches and described their importance. Subsequently, we studied global quenches starting from the free Hamiltonian to the interacting Hamiltonian with zero and non-zero background field. We computed the Loschmidt echo density and the expectation value of the chiral condensate density parameter and briefly commented of their dynamics. Also, we simulated a different global quench this time going from the interacting model with zero background field to the interacting model with non-zero background field. In this context, we studied the Loschmidt echo density and the dynamics of the axial fermion density and chiral condensate density parameters which were interesting since we know from chapter one the model shows critical behavior whenever $\mathcal{E}_0 = 0.5$. All three of this quantities showed oscillatory behaviors that we trace back to the dynamics of pair production due to the background electric field.

5

Discussion and outlook

In this thesis, we studied the Schwinger model both in its continuum and discrete lattice versions. We obtained various important and interesting results both theoretically and numerically regarding the chiral anomaly, the spectrum and the dynamics of the model.

We expressed the lattice version of the Schwinger model as a spin chain model with long-range spin-spin interactions modeling Coulomb's law. We studied the free massless, free massive and fully interacting models numerically using the exact diagonalization method. This was programmed in python using the package Quspin. We computed the ground state energy density, the gap energy, the chiral condensate density order parameter, and the axial fermion density order parameter. In particular, these order parameters were studied in the presence of a background electric field which induces a critical behavior in the system as a consequence of the dynamics

of pair production in one spatial dimension. Finally, some simple global quantum quenches were simulated and the Loschmidt echo density and the chiral density parameter and axial fermion density parameter were studied in this non-equilibrium context.

Perhaps the most natural continuation of this work should be towards studying more realistic gauge theories such as QCD using the same methods outlined in this work. It is important to note that we benefited greatly from working in 1+1 dimensional space, and higher dimensional theories carry more difficulties an subtleties. Another possibility instead of increasing dimensionality could be to consider another gauge theory with a different gauge group. The Schwinger model being an abelian $U(1)$ theory is the simplest gauge theory and perhaps the introduction of a non-abelian theory can shed light into novel and interesting results. Finally, we could think of continuing the venture along out of equilibrium dynamics of the Schwinger model. In particular, exploration of so-called dynamical phase transitions induced by quench dynamics in the Schwinger model. There is still a lot of ground to cover and the model despite its simplicity is full of interesting physics and neat, unexpected results.

References

[1] J. Schwinger. Gauge invariance and mass. II. *Physical Review*, 128(5):2425–2429, Dec 1962.

[2] J. H. Lowenstein and J. A. Swieca. Quantum electrodynamics in two dimensions. *Annals of Physics*, 68(1):172–195, 1971.

[3] C. Adam, R. A. Bertlmann, and P. Hofer. Overview on the anomaly and Schwinger term in two-dimensional QED. *La Rivista Del Nuovo Cimento Series 3*, 16(8):1–52, 1993.

[4] E. Abdalla, M. C. B. Abdalla, and K. D. Rothe. *Non-perturbative methods in 2 dimensional quantum field theory*. World Scientific, Singapore River Edge, NJ, 2001.

[5] S. Coleman. More about the massive Schwinger model. *Annals of Physics*, 101(1):239–267, sep 1976.

[6] J. S. Bell and R. Jackiw. A PCAC puzzle: $\pi_0 \to \gamma\gamma$ in the σ-model. *Il Nuovo Cimento A*, 60(1):47–61, mar 1969.

[7] S. L. Adler. Axial-vector vertex in spinor electrodynamics. *Phys. Rev.*, 177:2426–2438, Jan 1969.

[8] M. D. Schwartz. *Quantum Field Theory and the Standard Model*. Cambridge University Press, 2013.

[9] K. Fujikawa. Erratum: Path integral for gauge theories with fermions (Physical Review D). *Physical Review D*, 22(6):1499, sep 1980.

[10] M. F. Atiyah and I. M. Singer. The index of elliptic operators on compact manifolds. *Bulletin of the American Mathematical Society*, 69(3):422–434, may 1963.

[11] J. Schwinger. On gauge invariance and vacuum polarization. *Phys. Rev.*, 82:664–679, Jun 1951.

[12] W. Heisenberg. Zur Theorie des Ferromagnetismus. *Zeitschrift für Physik*, 49(9):619–636, sep 1928.

[13] H. Bethe. Zur theorie der metalle. *Zeitschrift für Physik*, 71(3-4):205–226, mar 1931.

[14] E. Lieb, T. Schultz, and D. Mattis. Two soluble models of an antiferromagnetic chain. *Annals of Physics*, 16(3):407–466, 1961.

[15] T. W. Ruijgrok and T. Niemeijer. The classical one-dimensional Heisenberg magnet in an external magnetic field. Transfer matrix formalism as an application of renormalization group theory "avant la lettre". *Physica A: Statistical Mechanics and its Applications*, 84(2):336–349, 1976.

[16] E. Barouch, Barry M. McCoy, and M. Dresden. Statistical mechanics of the XY model. i. *Phys. Rev. A*, 2:1075–1092, Sep 1970.

[17] E. Barouch and B. M. McCoy. Statistical mechanics of the *xy* model. ii. spin-correlation functions. *Phys. Rev. A*, 3:786–804, Feb 1971.

[18] G. Vidal, J. I. Latorre, E. Rico, and A. Kitaev. Entanglement in quantum critical phenomena. *Phys. Rev. Lett.*, 90:227902, Jun 2003.

[19] C. H. Bennett and D. P. DiVincenzo. Quantum information and computation. *Nature*, 404(6775):247–255, mar 2000.

[20] J. B. Kogut and L. Susskind. Hamiltonian formulation of Wilson's lattice gauge theories. *Physical Review D*, 11(2):395–408, 1975.

[21] L. Susskind. Lattice fermions. *Physical Review D*, 16(10):3031–3039, nov 1977.

[22] T. Banks, L. Susskind, and J. Kogut. Strong-coupling calculations of lattice gauge theories: (1 + 1)-dimensional exercises. *Phys. Rev. D*, 13:1043–1053, Feb 1976.

[23] T. M. R. Byrnes, P. Sriganesh, R. J. Bursill, and C. J. Hamer. Density matrix renormalisation group approach to the massive Schwinger model. *Nuclear Physics B - Proceedings Supplements*, 109(1):202–206, 2002.

[24] C. J. Hamer, Z. Weihong, and J. Oitmaa. Series expansions for the massive Schwinger model in Hamiltonian lattice theory. *Physical Review D - Particles, Fields, Gravitation and Cosmology*, 1997.

[25] P. Weinberg and M. Bukov. QuSpin: a Python Package for Dynamics and Exact Diagonalisation of Quantum Many Body Systems. Part I: spin chains. 2017.

[26] P. Weinberg and M. Bukov. QuSpin: a Python Package for Dynamics and Exact Diagonalisation of Quantum Many Body Systems. Part II: bosons, fermions and higher spins. 2018.

[27] R. B. Lehoucq, D. C. Sorensen, and C. Yang. *Arpack User's Guide: Solution of Large-Scale Eigenvalue Problems With Implicityly Restorted Arnoldi Methods*. Society for Industrial and Applied, 1998.

Colophon

This thesis was typeset using LaTeX. A template, which can be used to format a thesis with this look and feel can be found online at github.com/suchow/.